JOURNAL OF GEOPHYSICAL RESEARCH, VOL. 105, NO. D19, PAGES 24,409–24,429, OCTOBER 16, 2000

# Radiative impact of the Mount Pinatubo volcanic eruption: Lower stratospheric response

S. Ramachandran,[1,2,3] V. Ramaswamy,[1,4] Georgiy L. Stenchikov,[2] and Alan Robock[2]

**Abstract.** Volcanic aerosols in the stratosphere produce significant transitory solar and infrared radiative perturbations, which warm the stratosphere, cool the surface and affect stratospheric circulation. In this study, using the Geophysical Fluid Dynamics Laboratory SKYHI general circulation model (GCM) with a high vertical resolution and a recently improved radiative transfer code, we investigate the aerosol radiative forcing and the stratospheric temperature response for the June 15, 1991, Mount Pinatubo eruption, the most well observed and largest volcanic eruption of the 20th Century. The investigation is carried out using an updated, comprehensive monthly and zonal-mean Pinatubo aerosol spectral optical properties data set. While the near-infrared solar spectral effects contribute substantially to the total stratospheric heating due to aerosols, over the entire global domain the longwave component exceeds the solar in causing a warming of the lower stratosphere (30-100 hPa). In contrast, the magnitude of the solar perturbation (increased reflection) in the overall surface-atmosphere radiative heat balance exceeds that due to the longwave (infrared trapping effect). The troposphere affects the stratospheric radiative forcing, mainly because of the dependence of the reflected solar and upward longwave radiation on cloudiness, and this adds to the uncertainty in the calculation of the stratospheric temperature response. A four-member ensemble of 2-year GCM integrations (June 1991 to May 1993) were performed using fixed sea surface temperatures and a cloud prediction scheme, one set with and another without the volcanic aerosols. The temperature of the tropical lower stratosphere increases by a statistically significant 3 K, which is almost 1 K less than in previous investigations that employed coarser vertical resolution in the stratosphere, but is still larger than observed. In the low latitudes the evolution of the simulated temperature response mimics that observed only through about the first year. Thereafter, despite a significant aerosol optical depth perturbation in the tropical atmosphere, there is a lack of a signature in the temperature response that can be unambiguously attributed to the Pinatubo aerosols, suggesting other forced or unforced variations (e.g., ozone changes, quasi-biennial oscillation) occurring in the actual atmosphere which are unaccounted for in the model. In the high latitudes the large interannual variability prohibits a clear quantitative comparison between simulated and observed temperature changes and renders the aerosol-induced thermal signals statistically insignificant. In the global mean the evolution of the simulated lower stratospheric temperature response is in excellent agreement with the observation for the entire 2-year period, in contrast to the model-observation comparison at the low latitudes. This arises because in the global mean the stratospheric response is not sensitive to dynamical adjustments within the atmosphere caused by internal variations, and depends principally on the external radiative forcing caused by the aerosols.

## 1. Introduction

Major volcanic eruptions inject tens of megatons (Mt) of volatile gases and solid particles into the stratosphere. The large particles (mostly ash, consisting of silicate minerals) are 1 μm in diameter or more and rapidly settle out of the stratosphere. The principal volatile gases that influence the stratosphere are $H_2O$ and $SO_2$. Though large quantities of $CO_2$ are emitted during major volcanic eruptions, this source of carbon dioxide plays a minor role in the short-term global carbon budget and climate [*Turco et al.*, 1993]. The $SO_2$ molecules injected into the stratosphere condense and coagulate to form sulfate aerosols, typically in a few weeks after the eruption. These particles spread globally, with the dispersion depending on the latitude, altitude, and season of the volcanic injection and stratospheric transport processes. The location, time of the year, injection altitude, and the amount of $SO_2$ injected by the eruption are important in determining the eventual stratospheric aerosol particle size and amount and hence the global impact. The sulfate aerosols formed after the eruption scatter visible solar radiation back to space, leading to a cooling of the Earth's surface. They also absorb upwelling longwave radiation, warming the stratospheric layers where the particles reside, and thus provide a significant forcing of the climate system [*WMO*, 1990; *Houghton et al.*, 1996]. *Stenchikov et al.* [1998 (hereinafter referred to as S98)] showed that absorption of solar near-IR radiation contributes significantly to the stratospheric heating.

On June 15, 1991, the Mount Pinatubo (15.1°N, 120.4°E) eruption in the Philippines produced a major impact on the climate system. About 20 Mt of $SO_2$ were injected into the

[1]AOS Program, Princeton University, Princeton, New Jersey.
[2]Department of Environmental Sciences, Rutgers University, New Brunswick, New Jersey.
[3]Now at Physical Research Laboratory, Ahmedabad, India.
[4]NOAA Geophysical Fluid Dynamics Laboratory, Princeton, New Jersey.



Paper number 2000JD900355.
0148-0227/00/2000JD900355$09.00

stratosphere [*Bluth et al.*, 1992], which enhanced the global stratospheric aerosol mass loading [*McCormick and Veiga*, 1992]. For the first few months after the eruption the bulk of the material was confined over the tropics [*Trepte et al.*, 1993], from the tropopause level to about 28 km [*DeFoor et al.*, 1992]. After the Pinatubo eruption the tropical stratospheric aerosol optical depth at $\lambda$= 1.02 μm increased by 2 orders of magnitude [*McCormick and Veiga*, 1992].

Global pyrheliometer observations of the solar fluxes at the surface after the eruption showed that the perturbations reached several watts per square meter for more than a year and caused a surface cooling of about 0.5 K [*Dutton and Christy*, 1992]. *Minnis et al.* [1993] determined a top-of-the-atmosphere global mean forcing about -3 W $m^{-2}$ for August-September 1991 using Earth Radiation Balance Experiment (ERBE) radiometer data. Other observations over the 1991-1992 period (not necessarily attributable entirely to the volcanic eruption) include heating of the stratosphere by 3-4 K [*Labitzke*, 1994], enhancement of the northern polar vortex, increasing of the Arctic Oscillation (AO) [*Thompson and Wallace*, 1998] circulation signal in the troposphere, and corresponding winter warming over continents in the northern high and middle latitudes [*Robock and Mao*, 1992, 1995; *Graf et al.*, 1993; *Kirchner et al.*, 1999 (hereinafter referred to as K99].

*Lacis et al.* [1992], with a one-dimensional radiative-convective model for global mean conditions, calculated a net radiative flux change of -3 W $m^{-2}$ at the tropopause and a stratospheric temperature change of 0.9 K for sulfuric acid aerosols of optical depth 0.1 at 0.55 μm. *Hansen et al.* [1992] estimated the global-mean climate forcing by Pinatubo aerosols using the GISS GCM and performed GCM simulations with three scenarios of aerosol opacity. They determined that the global-mean forcing peaked at about -4 W $m^{-2}$ in early 1992, which though transitory exceeded the present forcing because of the anthropogenic greenhouse gases that have been added to the atmosphere since the beginning of the industrial revolution. *Hansen et al.* [1993, 1996] and *Kodera* [1994] simulated the potential climate impact of the Pinatubo eruption in the stratosphere and troposphere, with a simplified global evolution of aerosol properties.

*Kinne et al.* [1992], using a two-stream radiative transfer model, determined the heating rates of Pinatubo aerosols in the tropical stratosphere and found the heating of the tropical lower stratosphere to be about 0.3 K/d, mainly due to the absorption of terrestrial infrared radiation. *Young et al.* [1994] simulated the dispersion of the Mount Pinatubo volcanic cloud in the stratosphere for the first few months after the eruption, using a combined three-dimensional stratospheric circulation model and aerosol microphysical/transport model. They found that radiative heating of the cloud due to the prescribed upwelling infrared radiation from the troposphere is an important factor affecting the transport.

S98 combined Stratospheric Aerosol and Gas Experiment (SAGE) II and Upper Atmospheric Research Satellite (UARS) observations to develop a time- and space-dependent set of aerosol spectral characteristics for 2 years after the June 15, 1991, Pinatubo eruption. Using this data set, they simulated the radiative forcing due to Pinatubo aerosols in the Max Planck Institute for Meteorology GCM (ECHAM4) [*Roeckner et al.*, 1996] and found that the calculated maximum aerosol radiative forcing is about -6 W $m^{-2}$ at the surface over large areas, while the near-IR forcing contributes substantially to stratospheric heating. *Andronova et al.* [1999 (hereinafter referred to as A99)] simulated the evolution of Pinatubo radiative forcing using the University of Illinois at Urbana-Champaign (UIUC) GCM [*Yang et al.*, 2000] and S98 aerosol parameters with a more refined radiative model, and also found that the aerosol forcing in the near IR contributes substantially to the total stratospheric heating. K99 used the same aerosol data set and simulated the climate change for the 2-year period following the Pinatubo eruption with the ECHAM4 GCM. They simulated a winter warming pattern in the troposphere similar to that observed. They also found that the temperature of the tropical lower stratosphere increased by 4 K, which is higher than in observations, probably because ozone and quasi-biennial oscillation (QBO) cooling effects were not considered. *Timmreck et al.* [1999] conducted Pinatubo simulations with improved vertical resolution and interactively transported aerosols using the middle atmosphere (MA) version of ECHAM4 (MA/ECHAM4) GCM, with parameterized aerosol radiative effects based on S98. These recent climate response studies with both versions of ECHAM4 were conducted with relatively low vertical resolution or a crude description of aerosol radiative effects. For example, the 19-layer tropospheric ECHAM4 contains only seven stratospheric layers, and both ECHAM4 and MA/ECHAM4 use a two-band solar radiative transport algorithm.

In this work we simulate the Pinatubo aerosol radiative forcing and climate response using the 40-level SKYHI GCM with aerosol radiative properties similar to those calculated by S98. The GCM (section 2) has higher vertical resolution than previous studies and uses recently developed improved shortwave and longwave radiative algorithms (section 3) which have been calibrated against "benchmark" solutions. We investigate whether the results obtained by K99 with a lower resolution (both in the vertical coordinate and in wavelength) are model-dependent. In this study we take advantage of the superior accuracy of SKYHI in the simulation of stratospheric radiative and dynamical processes and focus on the stratospheric thermal response. Section 4 discusses the updated aerosol data set. The contributions of visible, near IR, and longwave spectral bands to radiative forcing, including the effects due to tropospheric clouds, are assessed in section 5. The aerosol optical depths used in this study and the radiative forcings obtained are compared with measurements and other model estimates in section 6. The stratospheric thermal response obtained from the GCM simulations are analyzed and compared with observations in section 7. The latitude-height profiles of temperature changes obtained from simulations are also compared with observations. Simulations with only the shortwave effects of aerosols are considered in addition to the nominal one (i.e., with both longwave and shortwave) in order to isolate the relative roles of the two radiative components. Finally, the stratospheric thermal response and the radiative forcing are contrasted with the forcings produced due to stratospheric ozone trend of the 1980s (section 8). The conclusions from this study are presented in section 9.

## 2. SKYHI General Circulation Model

The SKYHI GCM is a 40-level finite-difference grid model [*Hamilton et al.*, 1995; *Schwarzkopf and Ramaswamy*, 1999], with the top level at about 80 km. The vertical spacing in the model increases with altitude from about 1 km in the troposphere to about 2 km in the stratosphere and about 3 km in the mesosphere. The latitude-longitude resolution used in this study is 3.0° x 3.6°. The GCM uses predicted clouds [*Wetherald and Manabe*, 1988]; each layer is assumed to be fully cloud covered when relative humidity predicted by the model is equal to 100%.

Clouds are grouped into three categories of radiative properties: high clouds between 10 and 440 hPa, middle clouds between 440 and 680 hPa, and low clouds between 680 and 1000 hPa. The optical properties of clouds are parameterized following *Slingo* [1989]. The effective radius is set to 10 μm. The optical depths at 0.55 μm for the high, middle, and low clouds are 1, 3, and 12, respectively. In the model the sea surface temperatures (SSTs) are prescribed at the climatological mean values, varying seasonally and with latitude and longitude. The SKYHI GCM has served as a basic tool for studying the troposphere-stratosphere-mesosphere system for the past two decades at the Geophysical Fluid Dynamics Laboratory and has been used successfully in studies of several middle atmospheric phenomena [*Fels et al.*, 1980; *Mahlman and Umscheid*, 1984; *Mahlman et al.*, 1994; *Ramaswamy et al.*, 1996]. *Hamilton et al.* [1995] present a more complete description of the basic SKYHI model's stratospheric climatology. For the first time here, the SKYHI GCM is employed to study the impact due to volcanic aerosols in the stratosphere.

## 3. Radiative Transfer Algorithms

The shortwave radiative-transfer algorithm in the GCM follows *Freidenreich and Ramaswamy* [1999], and the results are calibrated against "benchmark" calculations. The shortwave (SW) spectrum ranges from 0.17 to 4.0 μm and includes absorption by $CO_2$, $H_2O$, $O_3$, and $O_2$ and Rayleigh scattering. The shortwave spectrum is divided into 25 bands, 10 in the near-IR region (0.68-4.0 μm), 4 bands in the visible (0.4-0.68 μm), and 11 bands in the UV region (0.17-0.4 μm). The algorithm utilizes the delta-Eddington method [*Joseph et al.*, 1976] together with a suitable treatment of gaseous absorption in conjunction with an appropriate adding technique [*Ramaswamy and Bowen*, 1994].

The longwave radiative-transfer algorithm is described by *Schwarzkopf and Fels* [1991] and is based on the Simplified Exchange Approximation method. It has been recently improved [*Schwarzkopf and Ramaswamy*, 1999] to account for the effects of $CH_4$, $N_2O$, halocarbons, and the foreign-broadened $H_2O$ continuum. The longwave (LW) spectrum ranges from 4.55 μm to ∞ and accounts for absorption by $H_2O$, $CO_2$, $O_3$, $CH_4$, $N_2O$, and four halocarbons (CFC-11, CFC-12, CFC-113, and HCFC-22). The longwave gaseous and aerosol radiative properties are approximated over 8 spectral bands. Only absorption by aerosols (but not scattering) is considered in the longwave region. Thus the radiative transport with the time-dependent Pinatubo aerosol spectral radiative effects is approximated over the 33 bands, 25 in the shortwave and 8 in the longwave spectral regions. In these simulations the Pinatubo aerosols are input between 200 and 10 hPa, which is 11 vertical layers in the model with roughly a 2-km resolution.

## 4. Pinatubo Aerosol Radiative Characteristics

A computation of the radiative forcing by the Pinatubo aerosols requires spectral-, space-, and time-dependent aerosol radiative properties (extinction coefficient, single-scattering albedo, and asymmetry factor). We derived a zonal, monthly mean aerosol optical property data set for the 60 latitude grids of the GCM in the 25 SW bands and 8 LW bands for the 2-year period from June 1991 to May 1993, following S98. The aerosol properties were calculated using observations from a wide range of satellite instruments (SAGE II, Stratospheric Aerosol Measurement (SAM) II, Advanced Very High Resolution Radiometer (AVHRR), UARS) [*McCormick and Veiga,* 1992; *Stowe et al.,* 1992; *Lambert et al.,* 1993], lidars [*DeFoor et al.,* 1992; *Jäger et al.*, 1995], and balloons [*Deshler et al.,* 1993], which together yield information on the spatial and temporal evolution of Pinatubo aerosols.

The procedure of obtaining the aerosol spectral characteristics is explained in detail by S98. A brief description is in order here. The observed SAGE II aerosol extinction at 1.02 μm and the effective radii retrieved from the Improved Stratospheric And Mesospheric Sounder (ISAMS) instrument on UARS are the basis for the derivation. Mie theory, assuming a refractive index of 75% solution of sulfuric acid [*Palmer and Williams,* 1975] and a unimodal lognormal aerosol size distribution, is employed to calculate the aerosol single-scattering characteristics. Mie calculations were performed for 60 spectral intervals, chosen specifically for better approximation of the sulfate aerosol radiative properties, and then averaged appropriately over the model wave bands. For this band averaging, because of high spectral resolution, we did not use any weighting function as in S98. The interpolation of the aerosol extinction coefficients to the model vertical grid was performed such that the total aerosol optical depth at 1.02 μm is conserved. As a result of this conservation, the calculated aerosol optical depth reproduces exactly the SAGE II optical depth at 1.02 μm. The width of the aerosol size distribution was chosen to better fit the UARS-derived optical depth in the longwave region.

The calculated zonal, monthly mean aerosol optical depth at 0.55 μm from June 1991 to May 1993 for the present GCM grid structure is shown in Figure 1. The aerosol optical depth reaches 0.3 in the tropics during the first few months after the eruption; the bulk of the aerosol was then confined to the tropics. Then, the Pinatubo aerosol propagated to higher latitudes and it took about 6 months to cover the whole globe. The signal of the August 12, 1991, Mount Hudson eruption (45°S) is also evident. In the 30°-70°N latitude band, aerosol optical depth values have the same value as in the tropics during January-April 1992. About 2 years after the eruption the aerosol optical depth has decreased considerably in the tropics, to about 0.1, because of the decrease in the number of aerosol particles due to sedimentation and dispersion.

The latitude-time distribution of the optical depth looks similar to S98 (their Figure 3a) and A99 (their Figure 1a), but the values here are generally greater than S98 and closer to A99. This is mostly due to a more accurate conservation of the total aerosol optical depth at 1.02 μm, which was used both for this study and for the A99 computations but not for S98. The impact of this exact conservation is rather small at 1.02 μm but increases with decreasing wavelength and does become significant for 0.55 μm; this is because the extinction is larger at 0.55 μm than at 1.02 μm. This enhancement results in larger optical depths at 0.55 μm in the middle and high latitudes, as seen in Figure 1. These large optical depth values did not occur in S98 and arise due to a combined effect of model resolution and aerosol vertical distribution. Such large values in the higher latitudes do, however, appear in the Advanced Very High Resolution Radiometer (AVHRR) observations [see *Russell et al.*, 1996; S98, Figure 3b].

## 5. Radiative Forcing of the Pinatubo Aerosol Cloud

We performed eight 2-year experiments with seasonally varying climatological SSTs, four with the Pinatubo aerosol

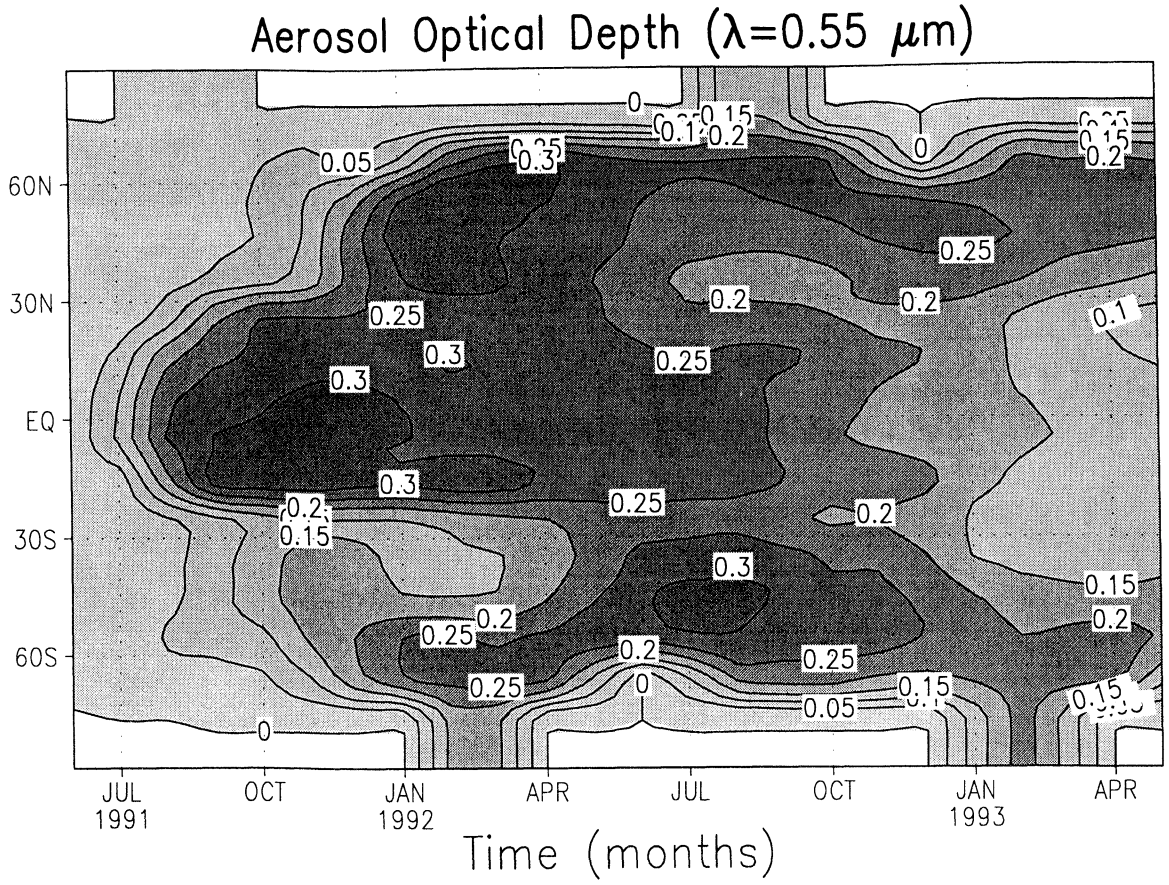


**Figure 1.** Calculated zonal, monthly mean, aerosol optical depth for 0.55 μm from June 1991 to May 1993 used in SKYHI simulations [from *Stenchikov et al.*, 1998]. See text for discussion.

perturbation and four without (control runs). The experiments were started with different initial conditions (same for the corresponding experiments with and without aerosols). The restart conditions were chosen arbitrarily from standard SKYHI GCM control experiments. Thus we obtained four statistically independent realizations for each case. The mean responses were evaluated by averaging the meteorological fields over the ensemble of four realizations. The statistical significance of the signals was also evaluated.

Using the fields from the control runs, we conducted off-line calculations of radiative fluxes and heating rates from June 1991 to May 1993, with and without stratospheric aerosols as in S98. The difference of radiative fluxes at the tropopause, computed with and without the aerosols and using the meteorological fields from the control run, is the aerosol radiative forcing of the atmosphere at any given time as per the definition of instantaneous radiative forcing [see *Houghton et al.*, 1996]. Two sets of calculations are performed, one for the total-sky (including cloudy and clear) conditions and one for clear-sky conditions. Note that our forcing definition at the tropopause differs from the so-called adjusted radiative forcing definition from *Houghton et al.* [1996]. In the case of stratospheric aerosols the differences between the two definitions are negligible [*Hansen et al.*, 1997]. We use the term "aerosol radiative forcing" here for instantaneous radiative flux and heating rate changes caused by aerosols at all model levels.

### 5.1. Perturbation of Top-of-the-Atmosphere Radiative Balance

Figure 2 shows clear- and total-sky zonal mean change of radiative fluxes caused by Pinatubo aerosols at the top of the atmosphere. The bands considered are the UV and visible (0.17-0.68 μm), near IR (0.68-4.0 μm), longwave (4.55 μm-∞), and total (integrated over the entire spectrum). For both solar and longwave, a downward flux is defined as positive (gain of energy by system) and an upward negative (loss of energy by system).

The solar forcings (visible and near IR) are negative (cooling of the system). The longwave forcing is positive at the top of the atmosphere and warms the system. The total Pinatubo radiative forcing is negative, indicating loss of energy from the Earth-atmosphere system. There is considerable spatial inhomogeneity, which varies with time, in turn giving rise to a temporal evolution in the strength of the meridional temperature gradient in the lower stratosphere. This feature is of considerable significance in the climate response [*Shindell et al.*, 1999]. Overall, the radiative forcing is confined within the tropics and subtropics until October 1991 [*Long and Stowe*, 1994]; then the aerosols and associated forcing spread to higher latitudes. A large clear-sky forcing starts in the equatorial latitudes during September 1991 and extends to April 1992.

There are four maxima in the visible and near-IR clear-sky forcings. The first is located in the tropics between September

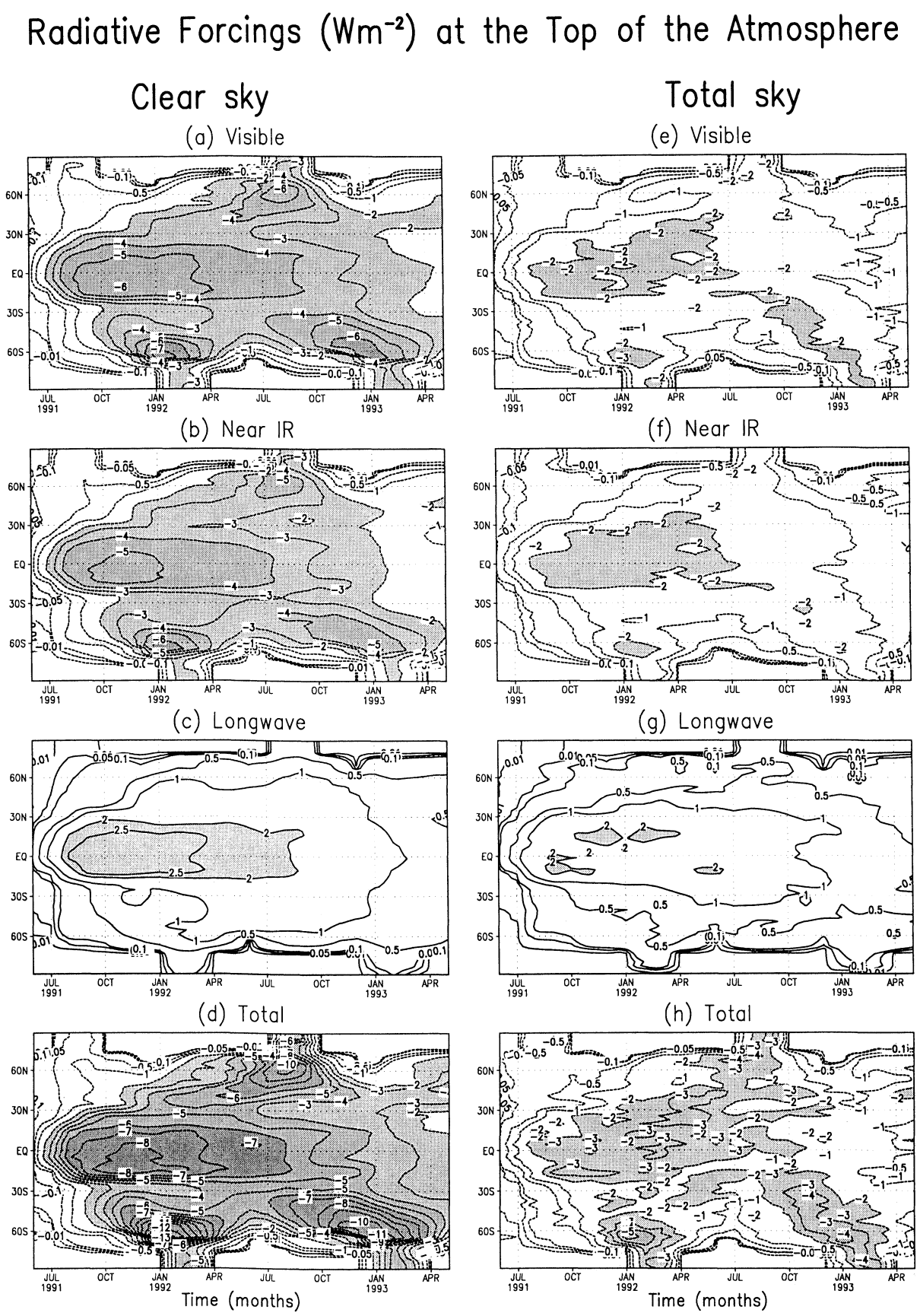


**Figure 2.** Zonally averaged radiative flux change (W $m^{-2}$) caused by Pinatubo aerosols at the top of the atmosphere from June 1991 to May 1993 for (a) visible (0.17-0.68 μm), (b) near-IR (0.68-4.0 μm), (c) longwave (4.55 μm-∞) spectral bands, (d) total (integrated over the entire spectrum) for clear-sky conditions, and (e, f, g, h) for total-sky. All flux changes are positive downward.

1991 and April 1992 and corresponds to the maximum aerosol optical depth there (Figure 1). The other three occur in spring and summer in high latitudes of both hemispheres. The variations in the radiative forcing follow the aerosol optical depth distribution and the seasonal variation of solar insolation. The clear-sky longwave forcing maximum, as the visible and near IR, is located in the 15°S-15°N latitude region and extends from September 1991 to April 1992.

The total forcing follows the solar forcing pattern and peaks at -8 W $m^{-2}$ at the top of the atmosphere in the tropics. The total radiative forcing is larger at the tropopause and surface (not shown) than at the top of the atmosphere. The clear-sky forcings in the visible and near IR are almost the same at all three levels, but the longwave forcing is largest at the top of the atmosphere and smallest at the surface.

Clouds reduce (e.g., S98) the visible and near-IR radiative forcing by about 2-3 W $m^{-2}$ (Figures 2e-2h) when compared with the clear-sky case (Figures 2a-2d). Model clouds reduce the longwave forcing by about 25% because of an effective screening of the emission from the surface and lower troposphere levels when compared to the clear-sky case [*WMO*, 1990; S98]. Thus the difference between the clear- and total-sky forcings is the largest in the areas with dense clouds, especially the equatorial region, and around 60° latitude in both hemispheres. The attenuation effect of clouds on the aerosol forcing in SKYHI calculations is stronger than in the simulations performed by S98 and A99 because the present model produces generally more cloud cover.

The total-sky longwave forcing at the top of the atmosphere is more than an order of magnitude higher than at the surface (not shown). As tropospheric water vapor, other trace gases, and clouds already absorb substantial LW radiation, there is only a small contribution by the LW to the total forcing at the surface. Both in clear-sky and total-sky conditions the magnitude of solar net flux change (solar forcing) always exceeds the longwave forcing, and hence the total forcing is negative.

Our results, in general, agree well with the model results of S98 and A99, but there are important quantitative differences. Our clear-sky forcings at the surface in the tropics are about 2 W $m^{-2}$ larger than S98 but are closer to A99 results. The possible reasons are as follows:

1. The aerosol optical depth calculations for SKYHI and in A99 are conducted with exact conservation of the observed total SAGE II optical depth for 1.02 μm. This causes an increase of the optical depth in the visible region and hence a difference relative to the calculations of S98 (see section 4). The averaging of aerosol radiative properties over the model spectral intervals in this study was conducted differently than in A99, because we did not use any weighting function, as discussed above.

2. S98 had two spectral intervals in the solar, one in the visible (0.25-0.68 μm) and one in the near IR (0.68-4 μm), and seven intervals in the longwave (3.56-250 μm). A99 had 11 bands in the solar, 8 bands for the UV and visible (0.175-0.7 μm) and 3 bands in the near IR (0.7-10 μm), and 9 bands in the longwave (3.33 μm-∞). In comparison, we have 25 bands in the solar, 15 bands in the UV and visible (0.17-0.68 μm) and 10 bands in the near IR (0.68-4 μm), and 8 bands in the longwave (4.55 μm-∞) to account for aerosols. Also in this study, aerosols are input between 200 and 10 hPa in 11 vertical layers of the model; this is in contrast to S98, who had a lower vertical resolution in the stratosphere [*Roeckner et al.*, 1996]. The finer spectral and vertical resolution may partially contribute to the forcing differences, as also observed by A99. Further, the benchmark-calibrated parameterization used in this study could be a reason for the differences with the previous models.

3. The treatment of cloud amounts and their radiative properties varies among the models, which would affect the total-sky forcings (see discussion by A99). Clouds in SKYHI reduce solar surface forcing more than in S98. Solar forcing from SKYHI is close to solar forcing from A99, but the longwave forcing from SKYHI is half of A99 and is close to S98.

### 5.2. Atmospheric Heating Rate Perturbations

Heating rate perturbation latitude-height cross sections are plotted in Figure 3. At the outset, in August 1991, the heating is confined to the tropics but then spreads to the higher latitudes of both hemispheres by January 1992. The heating in the vertical is spread between 100 and 5 hPa. Overall, the Pinatubo aerosol radiative effect is to cool the troposphere and substantially warm the stratosphere. The forcing in the UV and visible is limited to a small increase in heating in the upper stratosphere above the aerosol layer and a slight cooling below the top of the aerosol layer. The solar warming above the aerosol cloud is due to the absorption of enhanced reflected upwelling UV radiation by ozone and oxygen in the upper stratosphere, while the cooling in the aerosol layer is due to the backscattering of the direct incoming solar radiation and decrease of UV gaseous absorption in the aerosol layer. The reduction of the near-IR flux through aerosol backscattering of the incoming solar radiation cools the troposphere; this is quite substantial near the surface where near-IR absorption by water vapor is most significant.

Using an improved high spectral resolution radiative scheme in SKYHI, we found that the near-IR contribution to the solar forcing is substantial for the total stratospheric heating, as was first discussed by S98. It seems to be a robust effect because it was also confirmed by A99 in calculations with the UIUC GCM. In the longwave region, heating in the lower stratosphere is caused by the enhanced absorption of upward terrestrial longwave radiation by the aerosols. The maximum near-IR aerosol heating is at a higher altitude than the region of maximum longwave heating and reaches 0.1 K/d. The maximum LW heating is about 0.2 K/d. The maximum total (visible plus near IR plus longwave) aerosol heating is located at the 10-30 hPa level in the equatorial region, which is 10 hPa higher than in previous calculations with lower vertical resolution [S98]. It reaches 0.3 K/d, which agrees well with *Kinne et al.* [1992], S98, and A99. The heating is about 2 times larger than that estimated by *Shibata et al.* [1996] (see discussion by S98).

The longwave stratospheric cooling is substantial in the middle and high latitudes (Figure 3g). This cooling further adds to the warm-to-cool, equator-to-pole meridional heating perturbation initiated by the tropical lower stratospheric warming. This effect is larger in the present results than in S98 and A99. The reason for this stronger longwave cooling is the effect of high clouds on the upward LW flux. As a result, thermal emission by the aerosol layer is larger than absorption of the upward LW flux. We performed an auxiliary series of experiments where we removed different layers of clouds (low, middle, and high) from the model and studied the effect of the removal of the respective layers on the longwave heating rates. We found that when high clouds are removed, the large longwave cooling disappears. This shows that stratospheric radiative forcing is substantially sensitive to tropospheric conditions and cloud cover [see also *WMO*, 1990]. For the forcing at the top of the atmosphere, the solar dominates over the longwave. In the case of the lower stratospheric heating, the longwave dominates over solar at all except the high latitudes.

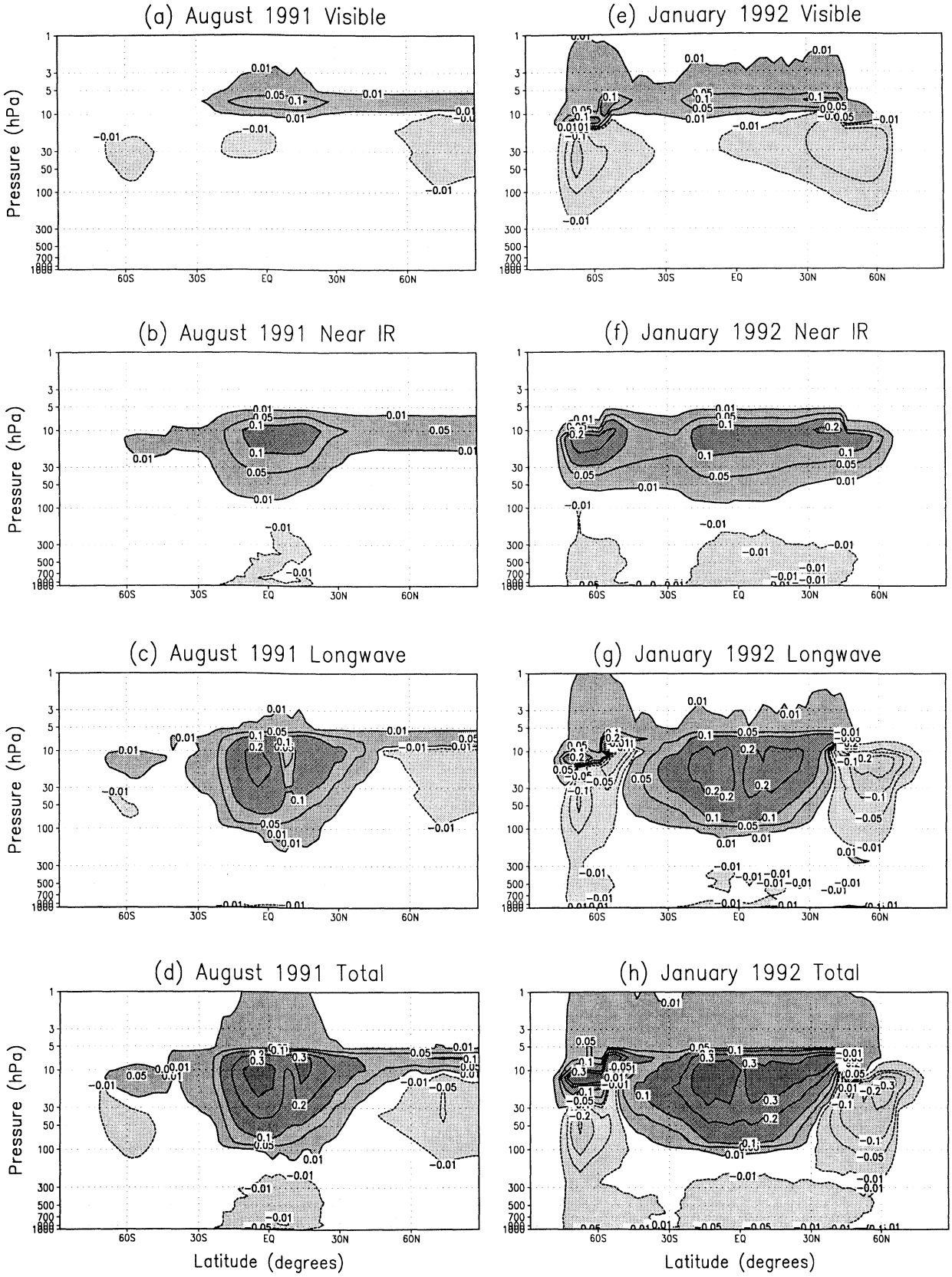


**Figure 3.** Zonally averaged perturbations of atmospheric heating rates (K/d) caused by the Pinatubo aerosols for August 1991 in the (a) visible, (b) near IR, (c) longwave, and (d) total, and for January 1992 in the (e) visible, (f) near IR, (g) longwave, and (h) total.

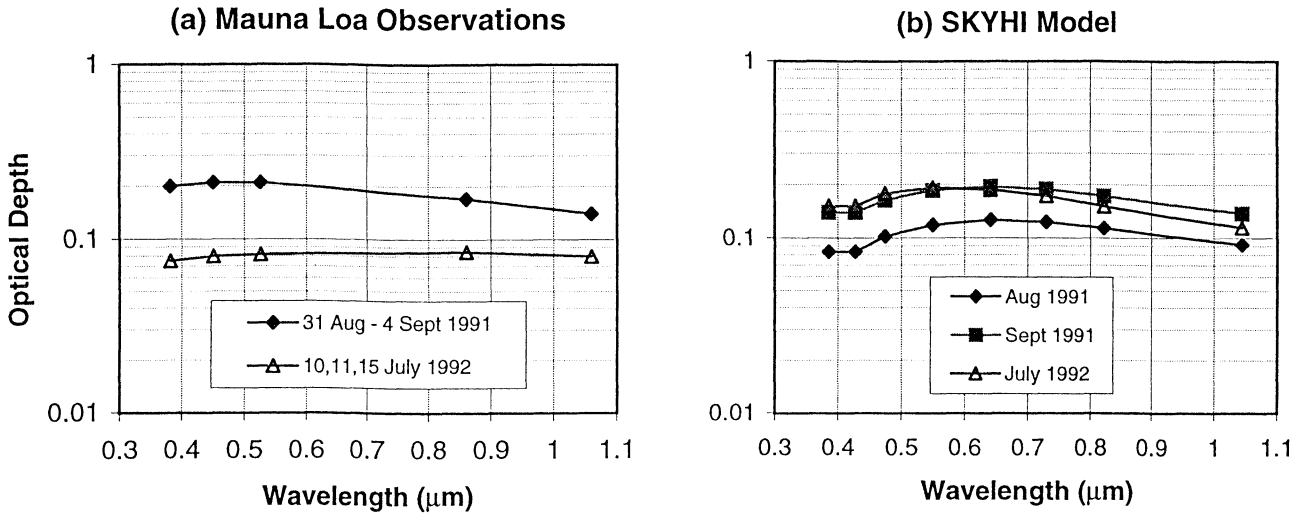


**Figure 4.** Aerosol optical depths in the 0.382 to 1.06 μm spectral band measured by (a) the Ames airborne tracking sun photometer [*Russell et al.*, 1993] at Mauna Loa, Hawaii, and (b) the aerosol optical depth values used in the SKYHI simulations at the same location.

However, near 10 hPa in the tropics the solar heating can yield as significant a contribution as the longwave heating.

## 6. Comparisons of the Pinatubo Forcing Estimates

In Figure 4, the monthly mean aerosol optical depths used in this simulation are compared with measurements made at Mauna Loa (19.5°N) [*Russell et al.*, 1993] for August and September 1991 and July 1992, over the spectral range 0.38-1.06 μm. During September 1991 the observed and calculated aerosol optical depths are quite similar. In July 1992 the observed optical depths are smaller than the aerosol optical depths used here. The differences could be related to sampling because the Mauna Loa measurements were taken near the edge of the dense part of the aerosol cloud where spatial and temporal variability is high. Therefore ground-based measurements of the optical depth are applicable for a day or, at most, a few days. The aerosol optical depths used in the GCM are derived from satellite monthly mean, zonally averaged global observations. During the initial period the vertical aerosol distribution was observed to be structured and inhomogeneous; initial inhomogeneities within the aerosol layer, which disappeared by early 1992, have been reported by *Deshler et al.* [1993] using balloon-borne optical particle counters over Laramie, Wyoming (41°N), *Shibata et al.* [1994] using a Nd:YAG lidar at Wakkanai, Japan (45°N), and *Jayaraman et al.* [1995] using a Nd:YAG lidar at Ahmedabad, India (23°N). In these measurements, the vertical aerosol profile showed a variation on a timescale of a few days.

*Russell et al.* [1993] used their measured aerosol optical depths to calculate the Pinatubo aerosol forcing for the months of September 1991 and July 1992. Using a two-stream model, resolving the solar spectral region into 8 bands and the infrared spectral region into 12 bands, and assuming a 55% cloud cover, they estimated the flux and heating rate changes due to the Pinatubo aerosols. The measured optical depth values for 0.55 μm are 0.21 (September 1991) and 0.10 (July 1992). In comparison, the aerosol optical depths used in the GCM are 0.185 and 0.191 during September 1991 and July 1992 for the location of Mauna Loa at 19.5°N (Figure 4).

It is interesting to compare the results from *Russell et al.* [1993] with our SKYHI simulations at 19.5°N for September 1991 (Table 1) when the aerosol optical depths in both studies are similar. *Russell et al.* [1993] used an effective radius of 0.56 μm and assumed column uniform aerosol properties, while in our study, aerosol varies with altitude and the column-average effective radius is about 0.5 μm. Larger aerosol particles absorb more in the LW.

**Table 1.** Comparison of Aerosol Optical Depths, Flux, and Heating Rate Changes from *Russell et al.* [1993] and the Results Obtained from the Present Study Using the SKYHI GCM for Total-Sky (left column) and Clear-Sky (right column), over Mauna Loa (19.5°N) for September 1991

| | *Russell et al.* [1993] | | | Present work (total/clear sky) | | |
|---|---|---|---|---|---|---|
| | Solar | Longwave | Total | Solar | Longwave | Total |
| Optical depth for 0.55 μm | 0.21 | | | 0.185 | | |
| Net flux change (W $m^{-2}$) | | | | | | |
| top of atmosphere | -6.2 | 4.5 | -1.8 | -3.8/-7.2 | 1.6/2.3 | -2.2/-4.9 |
| tropopause | -6.6 | 1.4 | -5.2 | -4.0/-7.4 | 0.6/0.7 | -3.4/-6.7 |
| Heating rate change (K/d) | | | | | | |
| for 22-23 km layer | 0.05 | 0.50 | 0.55 | 0.03/0.02 | 0.14/0.21 | 0.17/0.23 |

This shows that aerosol size distribution could affect the comparison with observations as well. The observed aerosol size distribution was polymodal, especially in the initial stages of the process, but converged to unimodal in about half a year. In our calculations we approximate the aerosol microphysical evolution with a unimodal size distribution. The results, discussed in detail by S98, show that in accordance with observations the column-average effective radius increases because of particle growth over the first 6 months and then decreases because of sedimentation.

*Russell et al.* [1993] report a higher solar heating (which could only be through near-IR absorption by aerosols) than in our calculations, but there is an even larger difference in the longwave and hence the total heating rates. An infrared heating of 0.50 K/d calculated by *Russell et al.* [1993] (compared to our 0.14 K/d) for September 1991 is too high in comparison with the results of all previous studies. The discrepancy in the radiative quantities is unlikely to be due solely to the possibility of different cloud amounts in the two models; there would have to be an extremely and unrealistically large difference in this parameter in order to lead to the dramatic disagreement seen in the longwave heating rates. The Russell et al. solar forcing values lie in between our clear and total-sky results. The differing treatment of aerosol infrared properties and transfer in the longwave in the two models are also likely important factors.

*Dutton and Christy* [1992] used the global pyrheliometer measurements at Mauna Loa to estimate a monthly mean clear-sky total solar irradiance decrease of approximately 5% after the Pinatubo eruption and 2.7%, on average, for the 10-month period following the eruption. This latter value corresponds to -10 W $m^{-2}$ clear-sky forcing at the surface (S98). The difference of solar fluxes in our runs with aerosols and without aerosols is -8 W $m^{-2}$ for the same place. The agreement between calculated and observed radiative forcing is reasonably good considering measurement errors and uncertainty in our calculations.

In Figure 5 the shortwave, longwave, and the net top of the atmosphere radiative flux changes between latitudes 10°S and 10°N are compared with ERBE satellite data [*Barkstrom*, 1984; *Minnis et al.*, 1993] for total-sky conditions. The ERBE wide-field-of-view data are available over the 11-year period from November 1984 to November 1995 (P. Minnis, personal communication, 1999). The observed fluxes, besides including the aerosol forcing effects, also account for changes in air, land, and sea surface temperatures, water vapor, cloudiness, and surface albedo. We calculated the monthly mean shortwave and longwave fluxes for the period 1984-1990 and then subtracted them from the 1991-1993 flux data to calculate the ERBE flux anomalies shown in Figure 5a. In Figure 5b we show the instantaneous aerosol forcing (i.e., the flux changes without considering the model's response) over a 2-year period; these were calculated using the control run fields as in Figure 2. The GCM flux changes in Figure 5c are averaged over the four ensemble runs with and without aerosols and hence include the model's atmospheric response caused by the aerosols. In particular, they include changes in air and land surface temperature, water vapor, and clouds. Figure 5d shows changes in cloud amount manifest in the model response. The ERBE flux anomalies are approximately mimicked by the forcing but differ from the more variable flux changes with model response considered. This is likely due to the cloud-induced variations differing between the model and the actual atmosphere.

Additionally, unaccounted for forcing could also be contributing to the differences in Figures 5b and 5c. The observed ERBE total-sky anomalies (Figure 5a) comprise not only the aerosol effects, expected to be large during the first few months, but also the effects due to other possible forcings, including consequences due to internal variability of the climate system. The net radiative perturbation is dominated by the SW through the summer of 1992.

The computed instantaneous forcing (Figure 5b) displays fewer variations than the observations. The SW component of the forcing increases from small values to about -5 W $m^{-2}$ in fall 1992 and then decreases much more gradually than observed, from a peak of -5 to -3 W $m^{-2}$ in October 1992. The discrepancy with respect to observations during the initial three months is likely because the model does not consider ash and other siliceous components that are a part of the volcanic injections but which tend to fall from the atmosphere within 2-3 months [*Turco et al.*, 1993; *Robock et al.*, 1995]. Thus although climatically not so important as the sulfuric acid aerosols, their signature would appear in the time series of the top of the atmosphere fluxes during the first few months. A similar explanation holds for the LW forcing because the ash particles have absorption bands in that part of the spectrum as well. Generally speaking, the computed forcings are similar to the observed anomalies, and the evolution after September 1991 in the SW, LW, and net forcing tracks the observed anomalies. The net forcing is slightly less than observed during the initial stages.

The evolution of flux changes taking into account the model's response (Figure 5c) matches the forcing qualitatively, but the flux changes are somewhat larger (especially the net forcing), indicating an amplification of the aerosol radiative perturbation. While the maximum departures from the control runs occur at approximately the same times as those in the forcing computation (fall 1991), there is a more pronounced oscillation evident particularly in the SW component. This occurs because of changes in cloud cover (Figure 5d), with an increase in winter 1992 and fall 1993 and a decrease in spring 1992. During the 2-year period the global aerosol optical depth has a smooth variation. Cloud increases cause an increase of the SW and LW anomalies, with the net dominated by the SW enhancement, and cloud decreases have the opposite effect. Thus cloud changes have the potential to yield quite large flux changes, at least in the present model run. This implies that it may be misleading to assume that the ERBE flux anomalies necessarily are representative of the aerosol forcing only, as has been assumed in a casual manner in some earlier studies. However, the cloud cover changes themselves in the present model may not be totally representative of the real atmosphere. More importantly, the cloud cover changes in Figure 5d are not statistically significant. This suggests that the flux changes in the model caused by cloud variations are also not statistically significant and makes it difficult to properly evaluate the effect of any aerosol-induced perturbations in cloud cover that may have occurred in reality and that may have altered the initial forcing values. This points to a difficult problem in evaluating model-observation comparisons of radiative flux changes for volcanic aerosols that have a limited duration. While *Mohnen* [1990] and *Sassen et al.* [1995] have discussed the possible effect of volcanic aerosols on seeding cirrus cloud formation, a global effect has not been quantified from observations, and the ERBE data show no identifiable signal.

With respect to the observed anomalies the model's flux changes evolve roughly in the same manner from September 1991 to April 1992 but with somewhat larger magnitudes. It is interesting to observe that the forcing calculation bears a closer resemblance to the evolution and magnitude ranges seen in the

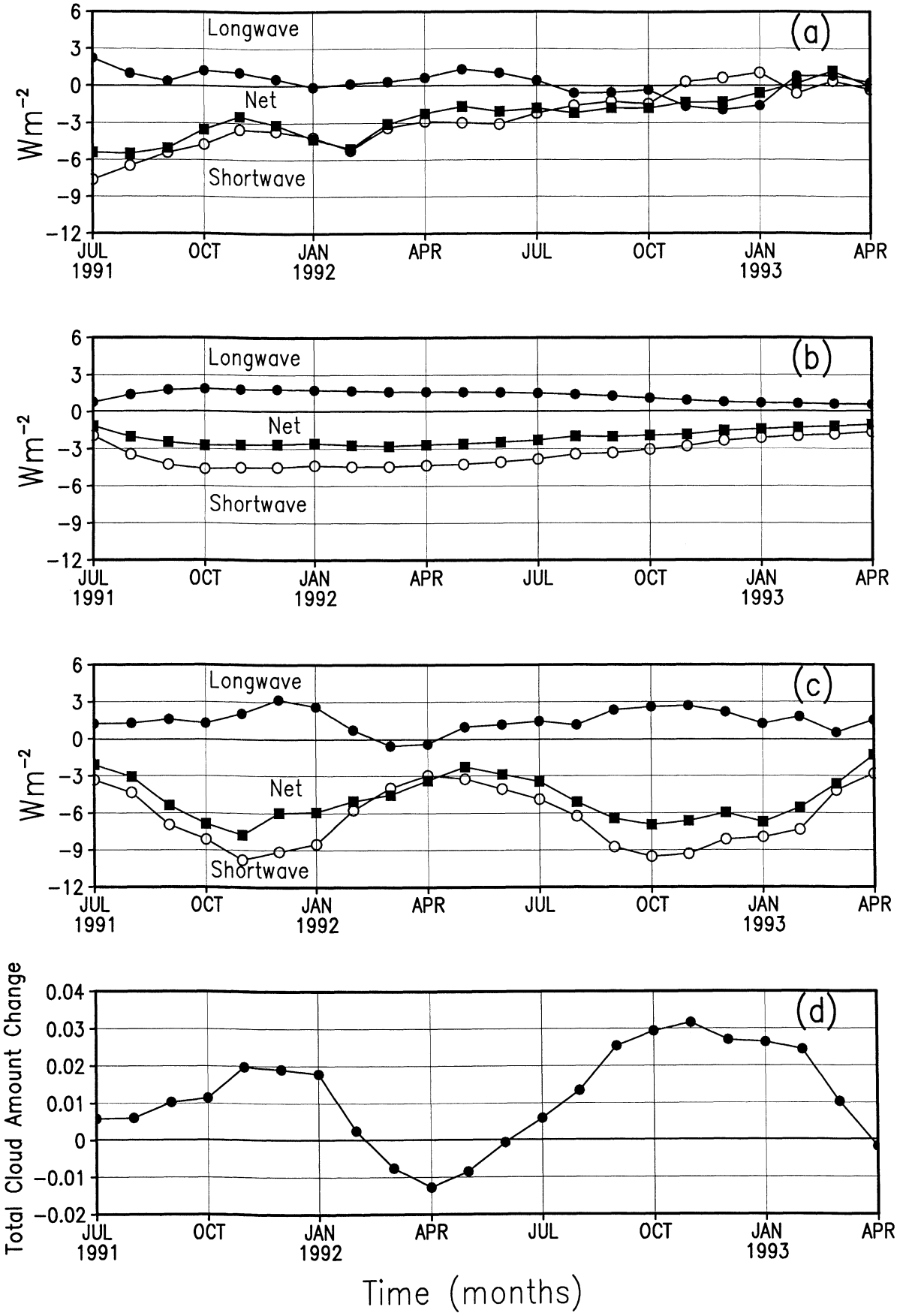


**Figure 5.** Three-month running mean shortwave, longwave, and net radiative flux perturbations averaged in the 10°S-10°N latitude band from (a) observed ERBE flux anomaly, (b) simulated radiative forcing, (c) simulated flux change, and (d) simulated cloud amount change (%) averaged in the 10°S-10°N band during July 1991 to April 1993.

observations than the flux changes, including the model's response. While this could be fortuitous, the similarity suggests that the specification of the aerosol space-time properties and the radiative forcing computation are quite reasonable. If there were no significant cloud cover changes in the model, then the simulated flux changes could track the observed pattern in a better manner. The lack of ERBE clear-sky data over this period inhibits a more quantitative assessment of the radiative role of clouds.

In the second year after the eruption, the computed forcing and the simulated flux changes in both observations and model become smaller, but the simulated flux changes are larger. One possible reason for the LW being larger than observed, even in the forcing computation, could be the QBO in 1992 (discussed later in section 7.1; Figure 7). The QBO is pronounced in the low latitudes and at that time caused an increase in the lower stratospheric temperature with respect to the climatological mean by ~1 K. This would cause the stratospheric layers to cool more to space and would serve to offset the anomaly due to the aerosols. As already noted, this effect is absent in the present simulations.

To compare our forcing estimates with the results of other calculations, we have linearly normalized our flux changes with respect to the spatially nonuniform aerosol optical depth to obtain the normalized total-sky solar $\Delta F_{Solar}/\tau_{0.55\ \mu m}$ and net $\Delta F_{Net}/\tau_{0.55\ \mu m}$ forcing at the tropopause for a uniformly distributed 0.55 μm optical depth $\tau_{0.55\ \mu m} = 0.1$ (Figure 6). We see that in general, during the 2-year period, $\Delta F_{Solar}/\tau_{0.55\ \mu m}$ is about -2 W m$^{-2}$, while the $\Delta F_{Net}/\tau_{0.55\ \mu m}$ is less due to the increase in the longwave flux and is in the range of –1 to –1.5 W m$^{-2}$.

The values obtained here differ from *Harshvardhan* [1979] and *Lacis et al.* [1992] results calculated for $\tau_{0.55\ \mu m} = 0.1$. *Harshvardhan* [1979] computed the forcings by introducing a uniform stratospheric aerosol layer over the globe. He calculated a solar and net forcing of about -4 and -3 W m$^{-2}$ on average, respectively, in the 60°S - 60°N latitude regions, assuming 75% sulfuric acid aerosols. Both the present and the *Harshvardhan* [1979] results indicate that the forcing per unit optical depth remains uniform in space and time. *Lacis et al.* [1992] computed the forcings for size distributions obtained during May and October 1982, about 1.5 and 6.5 months after the El Chichón eruption. They calculated a net forcing of -3 W m$^{-2}$ at the tropopause, using a one-dimensional radiative-convective model designed for global mean conditions.

The normalized forcing depends on the aerosol size distribution. It is larger for aerosols with median radii larger than 0.55 μm. The forcing is also sensitive to cloud amount and their optical properties. Errors of the delta-Eddington algorithm (used in SKYHI, S98, and A99) for reflection of a thin scattering layer could be as high as 20% [*King and Harshvardhan*, 1986; *Li and Ramaswamy*, 1996] and could contribute to the discrepancy of the results from different models. The aerosol radiative forcing calculated in this study is in reasonable agreement with the ERBE data (Figures 5a and 5b) especially considering the constraints noted earlier. The *Harshvardhan* [1979] and *Lacis et al.* [1992] radiative forcing, if scaled to the observed visible aerosol optical depth of 0.25-0.3, would be larger than in observations.

We calculate a global-mean net (solar and longwave) flux change for the 2-year period following the Pinatubo eruption of -2 W m$^{-2}$ at the top of troposphere. This transitory value can be compared to the estimate of +2-2.5 W m$^{-2}$ for the radiative forcing by today's levels of anthropogenic greenhouse gases (carbon dioxide, chlorofluorocarbons, nitrous oxide, and methane) since the industrial revolution [*Hansen and Lacis*, 1990; *Houghton et al.*, 1996]. By comparison, other natural and anthropogenic radiative forcings, such as solar irradiance changes or greenhouse gases, can alter the radiative forcing by only about 0.1 W m$^{-2}$ on a 2-year timescale [*Hansen et al.*, 1997].

## 7. Model Response to Pinatubo Forcing

An important objective of this study is to simulate and analyze the observed temperature response in the lower stratosphere due to the Pinatubo aerosol forcing. We compared the simulated system response with the National Centers for Environmental Prediction (NCEP) [*Kalnay et al.*, 1996] reanalysis data for the last 30 years from January 1968 to December 1997. We also analyzed the temperature data for the Northern Hemisphere at 30 and 50 hPa based on radiosonde observations obtained by the Free University of Berlin (FUB) Group [*Labitzke*, 1994], from January 1974 to December 1996. The NCEP reanalysis temperature fields were found to be in good agreement with the FUB data. As the NCEP data are available for both hemispheres, we use only their results for comparisons with simulations.

Figure 7 shows the zonally averaged 50 hPa temperature anomalies (from the simulation and NCEP reanalysis) in the period following the Mount Pinatubo eruption. A similar warming was found after the 1982 El Chichón eruption [*Angell*, 1997b; *Santer et al.*, 1999], but a detailed analysis is beyond the scope of this paper. The anomalies in the simulations were calculated with respect to the control and averaged for the four realizations. The anomalies from the observations (NCEP reanalysis) were calculated with respect to the 1986-1990 mean to account for the stratospheric temperature trend. The statistical significance of both observed and simulated temperature anomalies is determined for 90 and 95% significance levels and is shown in Figures 7a and 7b, respectively.

The temperature increases by about 2-3 K during the first half year following the eruption both in the simulation and reanalysis in the low latitudes. Each of the four ensembles yields approximately similar results, such that the mean temperature changes shown in Figure 7a represents well the changes to be expected in a general sense from the current model. In comparison, it should be borne in mind that the actual atmosphere has gone through only one particular realization and is represented here by the NCEP data. In this context the simulated statistical significance (or lack thereof) must be interpreted as indicative of the high probability of occurrence (or absence) of a robust aerosol-related signal in the temperature record. During the first northern winter, following the eruption, the simulated temperature responses are higher than observations, by about 1 K, in the 30°S-30°N latitude region. During the second winter the observed temperature anomalies are higher, being in the range of 2-3 K, than in simulations (which are about 1 K). Similar discrepancies between the observed and the simulated temperature responses were attributed by K99 to QBO and ozone depletion effects.

During the easterly phase of the QBO the stratospheric temperature at 50 hPa decreases in the tropics by about 1 K [*Angell*, 1997a, 1997b] and this leads to a decrease of the observed temperature anomaly. In November 1992 the equatorial winds shifted to a westerly phase and increased the observed temperature anomalies in the tropics. The NCEP data in Figure 7b suggest that this characteristic QBO effect is present in the observations throughout the period of our study.

The temperature changes shown in Figure 7, which are the mean of four ensemble anomalies, are statistically significant at a significance level of 90% or higher in the 30°S-30°N latitude

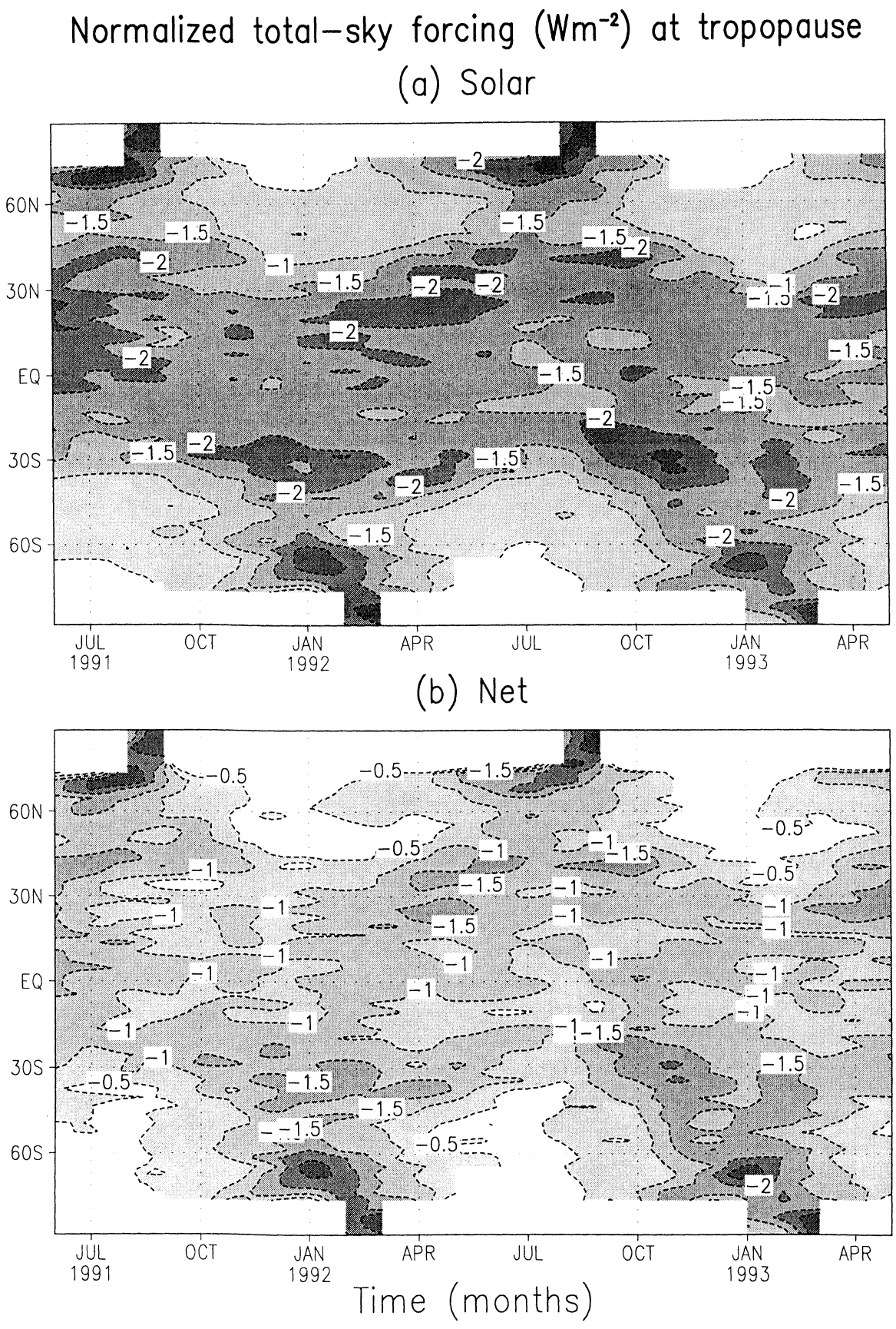


**Figure 6.** Simulated total-sky (a) solar and (b) net forcing at the tropopause normalized for aerosol optical depth of 0.1 at 0.55 μm.

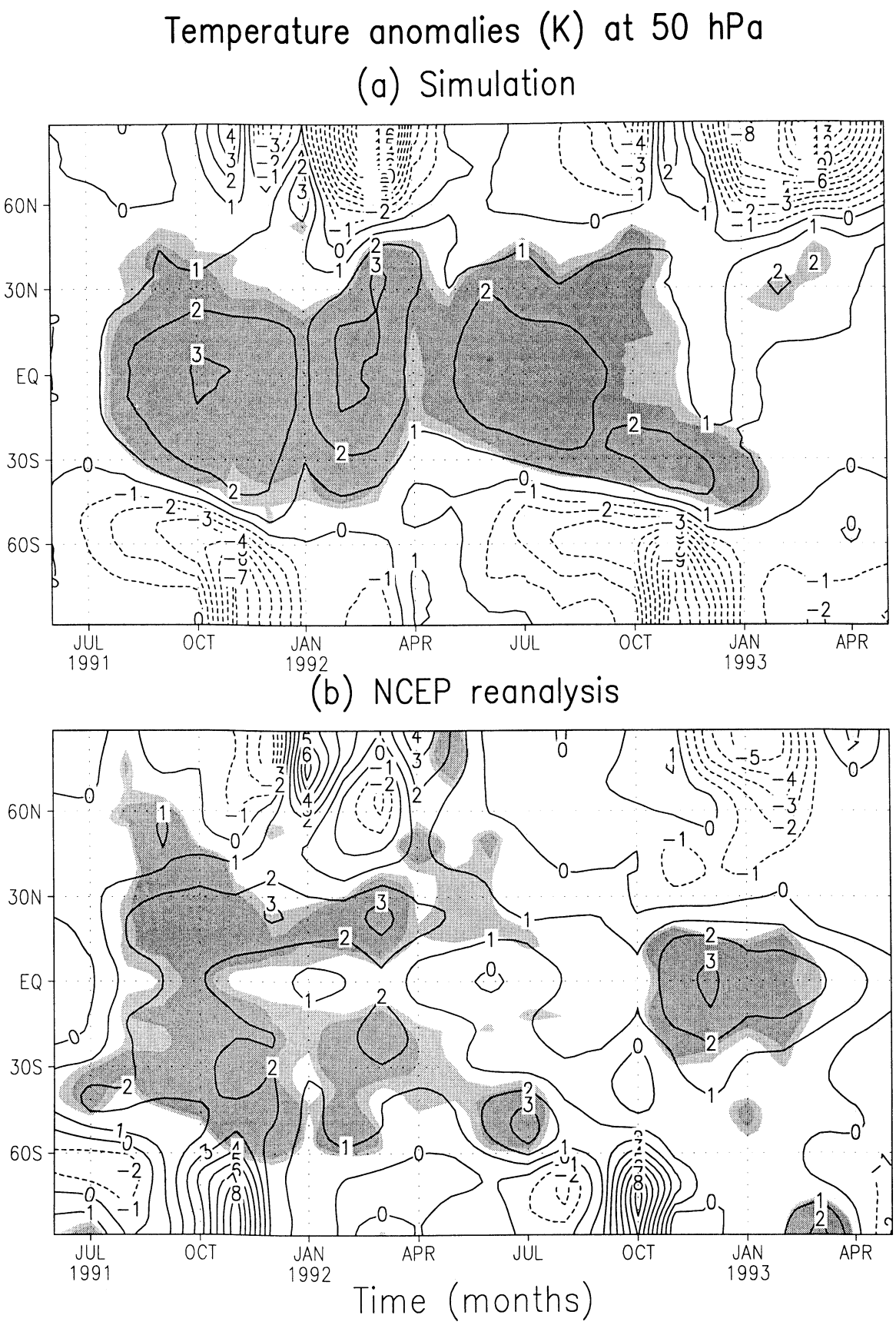


**Figure 7.** Latitude-time diagram of the zonally averaged anomalies (K) of lower stratosphere temperature at 50 hPa caused by Pinatubo aerosols: (a) simulated with climatological SSTs in the SKYHI GCM and (b) calculated from NCEP reanalysis data. The density of shading corresponds to 90 and 95% significance levels.

band. In the model the significance level of 90% or higher prevails until the 1992-1993 northern winter, but in the NCEP reanalysis, there is a gap in the manifestation of statistical significance during the northern summer of 1992. In the high and middle latitudes the model variability is higher and the signal-to-noise ratio is lower than in the reanalysis. The temperature changes at high latitudes fail the significance test due to the large interannual variability in those regions, a feature that is prevalent in observations [*Labitzke and van Loon*, 1995] and model simulations [*Ramaswamy et al.*, 1996; K99; *Schwarzkopf and Ramaswamy*, 1999], and could in part be due to insufficient ensemble statistics.

Figure 8a shows the evolution of the simulated and observed temperature anomalies at 50 hPa in the tropical region (10°S-10°N) where the QBO effect is pronounced. Although the simulated temperature anomalies are higher than observed because of QBO and ozone effects (K99), the variations are quite well correlated for about a year after the eruption. After June 1992, however, the simulated anomalies decrease but the observed anomalies go up reflecting a distinct signature of QBO. The NCEP temperature anomalies in Figure 8a were calculated with respect to both a 5- (1986-1990) and 24-year (1968-1997 excluding 1982-1984 and 1991-1993) mean to compare the amplitude of the stratospheric temperature trend (quite low in tropics) with the Pinatubo effect. The differences between the two computations involving the NCEP data are small.

The simulated temperature anomalies in Figures 7a and 8a are about 1 K less than in K99. This is likely due to the increase of the amount of (especially high) clouds in the runs with aerosols (Figure 5d), which tends to reduce the upward thermal flux and also decrease longwave and thus the net stratospheric heating. In addition, the core of maximum heating in the present model is ~10 hPa higher than in ECHAM4 model (S98), which can be expected to lead to a more efficient cool-to-space emission and cooling of the stratosphere. As the present SKYHI model has a higher vertical resolution than ECHAM4, vertical heat advection and stratosphere-troposphere exchange are probably described in a better manner.

Short-term ozone loss after a large volcanic eruption is caused by heterogeneous reactions on aerosol surfaces in the midlatitudes [*Hofmann and Solomon*, 1989; *Solomon et al.*, 1996; *Solomon*, 1999] and upward motion of tropospheric air into the stratosphere in the tropics [*Kinne et al.*, 1992]. Ozone depletion causes less UV absorption and could decrease the lower stratospheric temperature (K99). To estimate ozone effects in SKYHI, we conducted an offline fixed dynamical heating [*Fels and Kaplan*, 1975; *Ramanathan and Dickinson*, 1979; *Fels et al.*, 1980] calculation to determine the temperature change produced by the observed ozone depletion in 1991-1993. *Schoeberl et al.* [1993], *Herman and Larko* [1994], and *Randel et al.* [1995], using TOMS and SBUV2 measurements, found substantial decreases in column ozone (5-10%) over large regions of the globe during the 1991-1994 period, with strong variations in space and time. *Grant et al.* [1996], using ECC sonde data, found an 8% decrease of ozone between 16 and 28 km during the 1991-1993 time frame in the tropics. On the basis of the above measurements we introduced a 10% ozone depletion in the 16-28 km region. On average, we found a cooling of about 1 K in the tropics and midlatitudes in this altitude region. This corroborates well the K99 results of a tropical temperature decrease of about 1 K; however, it should be noted that fixed dynamical heating overestimates substantially the regional cooling that would be obtained by a GCM [*Ramaswamy et al.*, 1996]. The computed cooling effect due to the observed ozone changes are in the right direction toward explaining the slightly larger temperature change in the tropics obtained in the model relative to the observations.

Figure 8b contrasts the simulated and observed temperature responses at 50 hPa in the global mean, just as Figure 8a for the tropics. Each of the four ensemble members yields an excellent agreement in the evolution of the temperature perturbation. The difference in the amplitude of the peak with respect to observations in the first few months, when aerosol distribution was not yet stabilized, could be due to radiative effects (e.g., inaccuracies in aerosol property specifications). In 4-5 months, after the aerosols were distributed globally, the mean from the ensembles is not only in excellent agreement with observations but also tracks the global-mean values right through the full 2-year period. This is in contrast to the tropics, where after the spring of 1992, both the amplitude and the evolution of the temperature anomaly differ significantly from the observations. This divergence in the low latitudes occurs despite the fact that the aerosol optical depth at this time is more than 0.25 (equivalent to a global-mean forcing of -3 W $m^{-2}$ or more in magnitude), which may be construed as being a sufficiently large forcing capable of yielding a large temperature response in the observations that the model can capture; unfortunately, it appears that other factors, probably internal dynamical variations unaccounted for in the model, may have been even more dominant in the actual tropical atmosphere than the aerosol forcing.

The reason for the differing features in Figures 8a,b is because in the global-mean the temperature anomaly in the lower stratosphere, to a good approximation, is reflecting the effect of an externally (i.e., external to the climate system) imposed perturbation only. The global mean is considerably less sensitive to the effects of an internal adjustment within the climate system or a variability in the dynamics that has a necessarily non global character. Since dynamical features would nearly cancel in the global mean, Figure 8b is very likely manifesting an aerosol signal. The fact that there is good agreement (despite QBO and ozone cooling effect not accounted for) indicates that over the 2-year period the Pinatubo aerosol forcing was the most dominant external forcing mechanism. The agreement also indicates that the manner of representation of the forcing here (i.e., the space-time data, the radiation model, and the GCM) in the global-average situation is being handled well. The fact that Figure 8a does not replicate the global-mean features is indicative of a dynamical rearrangement within the stratosphere (most likely the QBO) which overrode the radiatively induced perturbation due to the aerosols in spite of the fact that the optical depths in the tropics were still quite high. Also, the lack of significance in the high latitudes implies that signals need not be detected there even if the aerosol optical depth perturbations are large.

Thus in the Pinatubo case, while there is confidence in the aerosol signature on the global lower stratospheric temperatures for two full years, that for the tropical regions is only till about the end of spring 1992 (or ~9 months after the eruption). It is possible that QBO influences could be contributing even during the first year after the eruption. For the high latitudes the plausible attribution of the temperature changes to Pinatubo aerosols is complicated through the 2-year period by the high variability there (Figure 7). While this inference could be model-dependent, it suggests that the estimate of duration of a detectable volcanic impact at specific latitudes must take into consideration the other forcings and internal variability of the climate system, besides the aerosol perturbation magnitude.

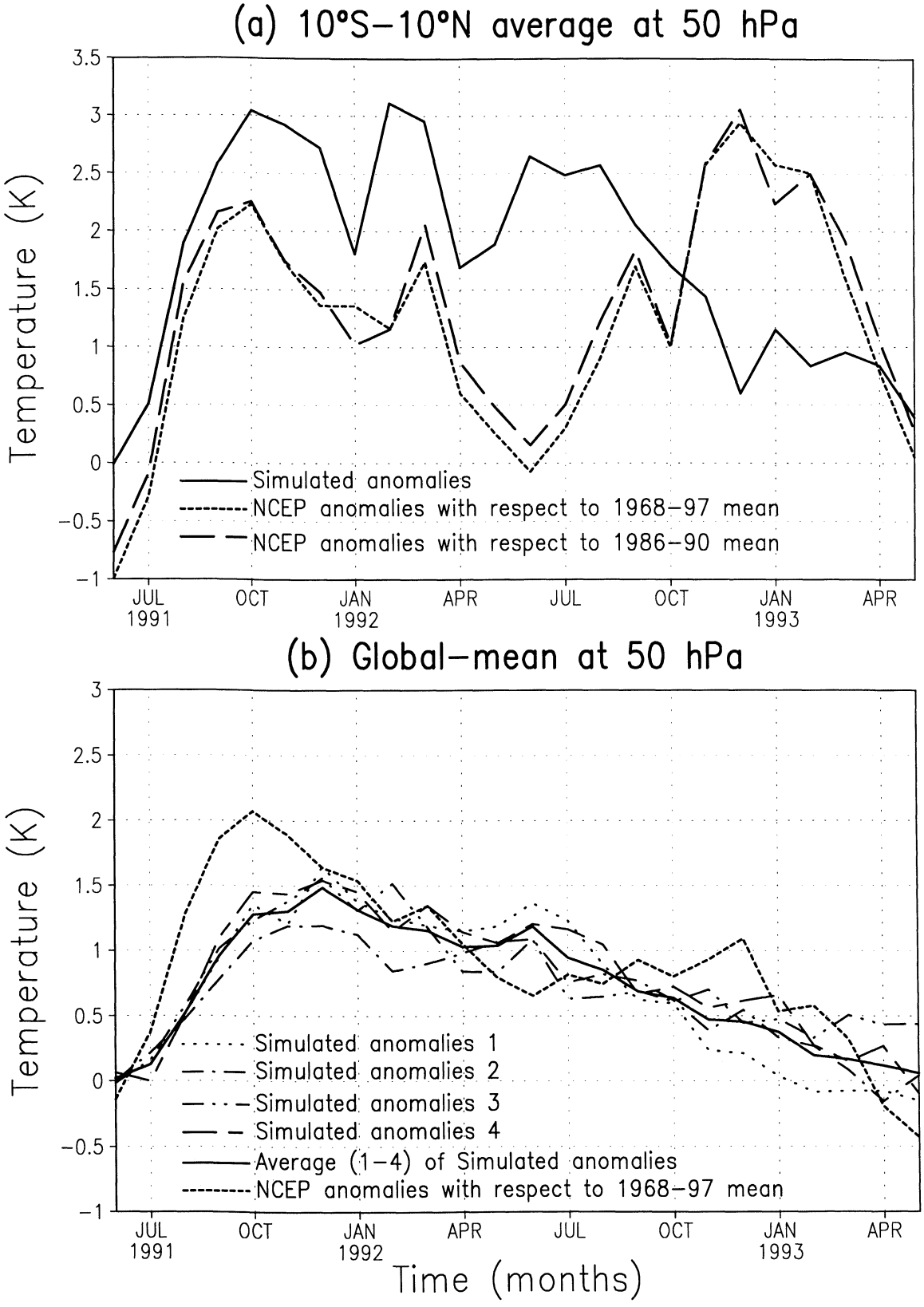


**Figure 8.** Lower stratospheric temperature anomalies (K) at 50 hPa caused by Pinatubo aerosols obtained from simulations and NCEP reanalysis averaged (a) in the latitude region 10°S-10°N and (b) globally. The simulated anomalies are calculated with respect to the control run. The NCEP anomalies are calculated with respect to 1968-1997 and 1986-1990 means, with the volcanic years of 1982-1884 and 1991-1993 removed.

The zonal-mean vertical structure of the atmospheric thermal response from our simulations and NCEP reanalysis is shown in Figure 9. A heating of 2-3 K is seen in November 1991 in the 50-10 hPa region, mainly in the 30°S-30°N latitude band. The large temperature fluctuations in the middle and high latitudes in both hemispheres reflect the large interannual variability in those regions. The stratospheric warming persists for about 1.5 years after the eruption. In May 1993, however, when the aerosol optical depth has decreased by a factor of 3 (Figure 1) from November 1991, we do not see a significant warming of the lower stratosphere in the model simulation. The area of significance for the ensemble-mean temperature change is larger than in observations, a feature seen for 50 hPa as well. In November 1992 in the equatorial region, the simulated temperature response is about 1 K in the 100-30 hPa region, while it is about 2 K in NCEP reanalysis. In May 1993, both simulations and NCEP reanalysis have very little "significance" area, reiterating that because of high internal variability in the particular pressure layers and latitude bands, there is less than a 2-year warming of the lower stratosphere that can be attributed to the aerosols (see also Figure 8). We see that in the 100-10 hPa region, as at 50 hPa, after about a year, the aerosol-induced signal has a high potential to be lost in meteorological "noise." While the radiative timescale of the stratosphere is relatively short, the climatic effects at the surface, where there are components of the climate system with longer memory (e.g., ocean, soil moisture, and snow), the effect of volcanic eruptions could persist for longer periods [*Robock*, 2000].

As we saw in Figure 3, the near-IR solar heating is significant and reaches 0.2 K/d. To determine the contributions to the temperature response produced by the shortwave and longwave effects individually, we performed an auxiliary ensemble of four experiments with the same SKYHI GCM. This set of experiments was aimed at calculating the temperature anomalies produced by the Pinatubo aerosols by considering their shortwave effects only. Figure 10 shows the evolution of zonal mean temperature anomalies at 50 hPa produced by only the shortwave effects of Pinatubo aerosols at 50 hPa. We see that the solar near IR absorption contributes to about a third of the total temperature anomaly. Thus the remaining 67% of the warming of about 2 K in the lower stratosphere comes from the absorption of thermal infrared by the volcanic aerosols. The effect of solar heating is more significant between 30 hPa and 10 hPa where it is maximized.

## 8. Stratospheric Aerosol Increases Versus Stratospheric Ozone Depletion

A large volcanic eruption can cause a climate forcing which significantly dominates other global radiative forcings for 1-2 years following the eruption [*Hansen et al.*, 1997]. Here we compare the volcanic aerosol forcing and impacts with another important stratospheric forcing, namely the long-term stratospheric ozone trend. In Figure 11 the 2-year mean temperature change produced by the Pinatubo eruption is contrasted with the annual-mean temperature change produced by the 1979-1990 observed global ozone losses between 400 and 25 hPa in the SKYHI GCM [*Ramaswamy et al.*, 1996]. Warming due to aerosols and cooling due to ozone is found above 100 hPa, where principal ozone losses occur. The peak warming is about 2 K in the 2-year mean temperature change, while the cooling due to ozone is only about 0.5 K in the tropics. While the warming due to Pinatubo is concentrated in the tropics (30°S-30°N), where the bulk of the aerosols were found after the eruption, the peak cooling due to ozone is about 1 K in middle and high latitudes where the maximum ozone losses occur. The global, annual-mean GCM temperature change due to the ozone losses for 11 years (1979-1990) in the 100-50 hPa (~ 16-21 km) lower stratospheric region was found to be -0.6 K [*Ramaswamy et al.*, 1996]. The global, 2-year mean GCM temperature change due to Pinatubo aerosols is found to be 0.3 K in the same altitude range. Although the volcanic aerosol changes are transitory, they can dominate the stratospheric temperature impacts due to other global radiative forcings over the limited period of their duration. As discussed in section 8, the volcanic aerosol effects neglect volcanic perturbations to ozone.

In Table 2 we compare the Pinatubo aerosol forcing at the tropopause with the forcing caused by the stratospheric ozone trend [*Ramaswamy et al.*, 1992] for various latitude bands. Since the forcings due to observed ozone losses are for the 11-year period of 1979-1990, the aerosol forcings have also been scaled to the 11-year period by multiplying by 2/11. The Pinatubo aerosol forcing is a maximum in the tropics and decreases toward the poles. The forcing due to ozone losses is maximum in the 60°-90°S belt, while in the 90°-60°N regime, its value is halved. In the tropical regime, between 10°N and 30°S, the ozone forcing is zero, because there is no ozone trend in this latitude range. On a global-mean and quasi-decadal scale the forcing due to ozone trend is -0.08 W $m^{-2}$ and is about 5 times less than the Pinatubo aerosol forcing. Thus we see that the spatial distribution of simulated radiative forcing and the lower stratospheric thermal response caused by stratospheric aerosols and ozone trend are quite different.

## 9. Conclusions

This study has investigated the radiative forcing and stratospheric thermal response of the GFDL SKYHI GCM to the Pinatubo volcanic eruption, using the observed aerosol optical properties as input. The calculations were performed with an improved radiation algorithm and with better vertical and spectral resolution than used in several earlier studies. The stratospheric response is determined by running an ensemble of four GCM runs involving integrations over the period from June 1991 to May 1993. Our calculations confirm that the near-infrared solar forcing contributes substantially to the total stratospheric heating following a large tropical volcanic eruption. The increase in the solar radiation absorbed by ozone owing to the enhancement in scattering caused by aerosols is confined to the top layers (10 hPa and above); the near-IR absorption extends downward to 50 hPa. Longwave aerosol absorption is spread throughout the depth of the aerosol layer, with a peak at 20-30 hPa. The solar near-IR heating accounts for a third of the thermal response in the lower stratosphere, with the longwave heating effect providing the rest. In contrast, the magnitude of the solar reflection exceeds the longwave greenhouse effect in terms of the forcing of the surface-troposphere system. The tropospheric cloud distributions affect the stratospheric radiative perturbations in both solar and longwave, and this introduces uncertainties in the stratospheric thermal response. Our clear-sky forcing is in fair agreement with earlier studies.

A comparison of the optical depth used here with the Mauna Loa Sun photometer measurements indicates a fair agreement. The small difference is probably due to the differences in time and space sampling between the essentially satellite-based data used here and the ground-based measurements. The small

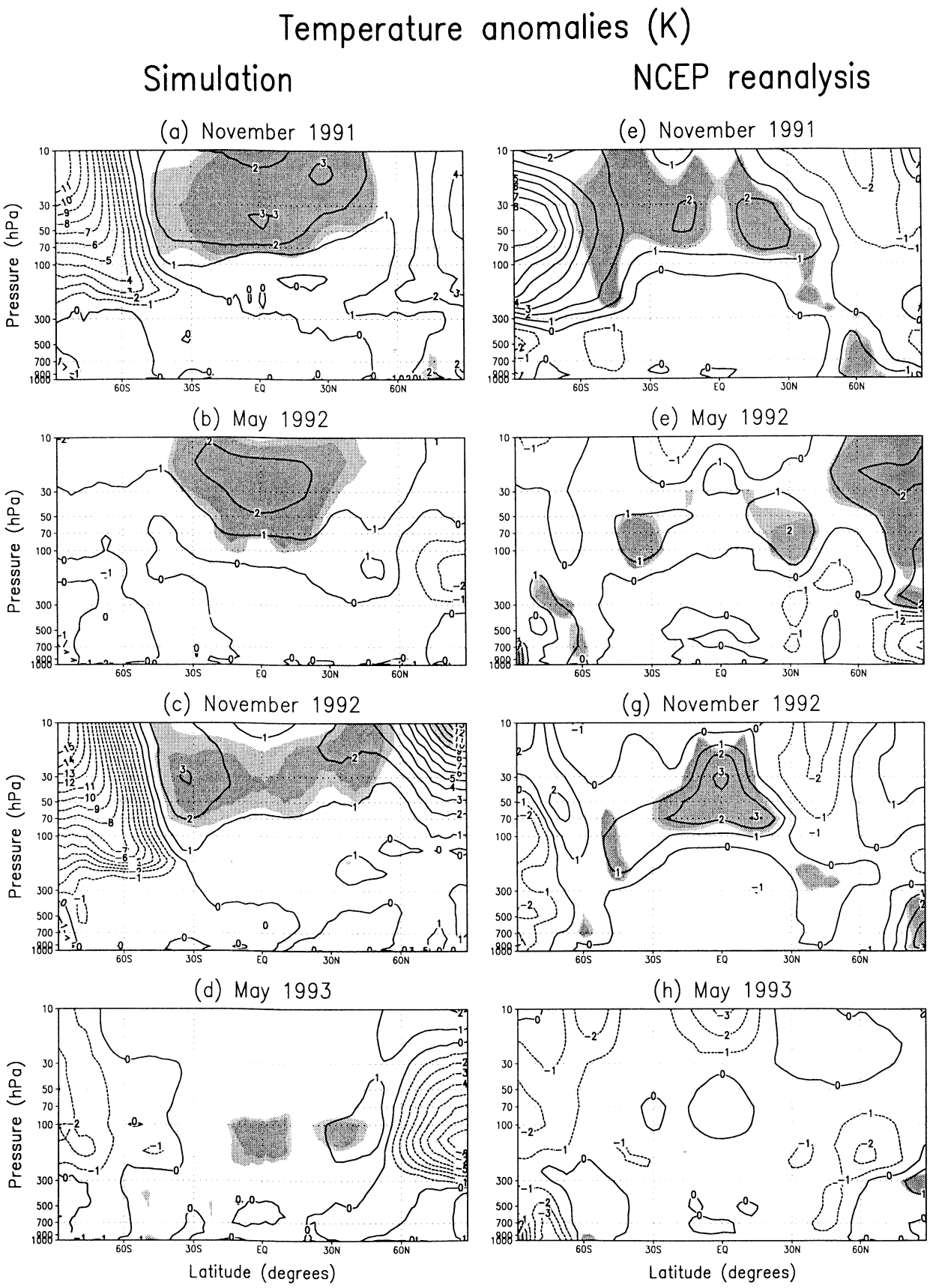


**Figure 9.** Latitude-height distributions of zonal-mean temperature anomalies (K) obtained from SKYHI simulations (mean of the ensemble runs): (a) November 1991, (b) May 1992, (c) November 1992, and (d) May 1993, and (e, f, g, h) from NCEP reanalysis for the same times. The density of shading corresponds to 90% and 95% significance levels obtained by a Student's *t*-test.

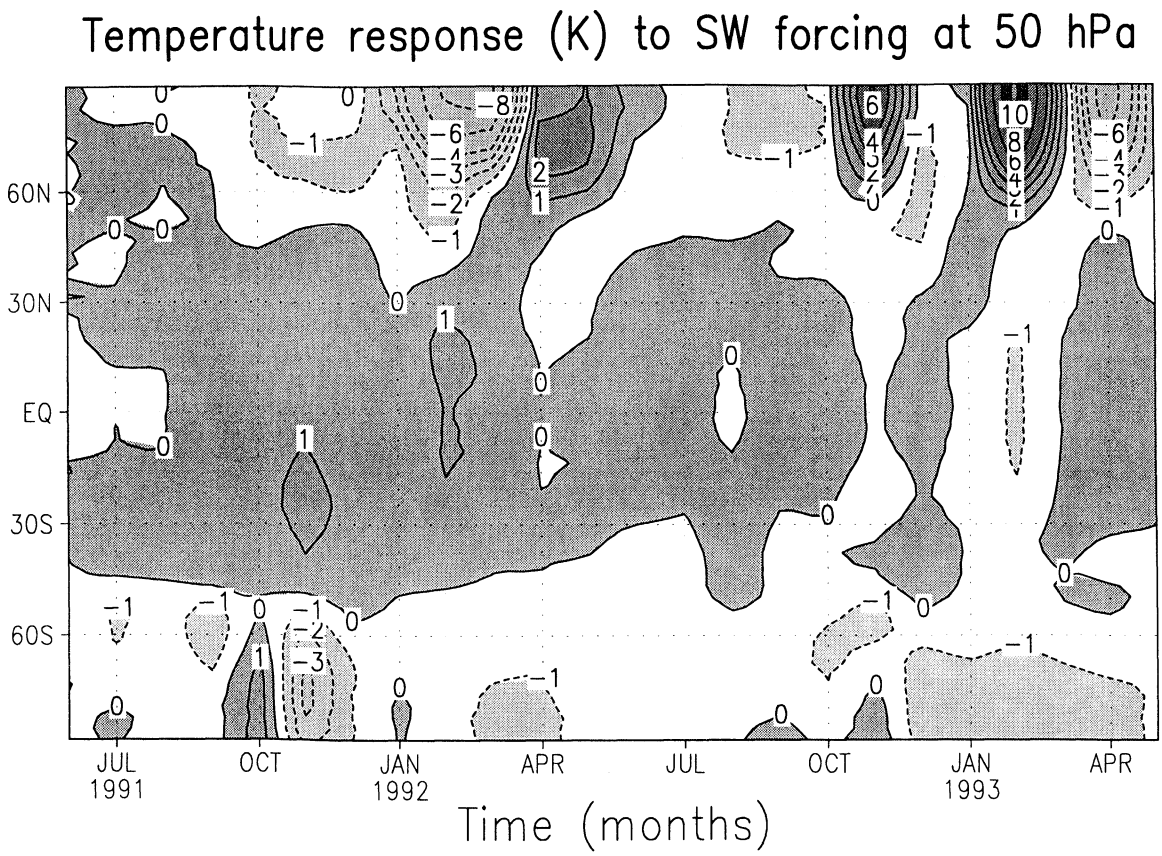


**Figure 10.** Latitude-time diagram of the zonally averaged temperature anomalies (K) at 50 hPa produced due to only the shortwave effects of the Pinatubo aerosols.

difference in optical depth would imply a reasonable correspondence in the clear-sky forcing. However, comparison with an earlier model study that used ground-based optical depth measurements indicates disagreements in the forcing, likely arising due to differences in the radiative transfer treatment and cloud cover assumptions.

In comparison with the ERBE TOA radiation budgets, our total-sky net radiation forcing is within 1 to 2 W $m^{-2}$ for most of the time duration (2 years) of the aerosols. When compared with the fluxes emerging from the model's response, the simulated values are even more different from the observation. The model's response in TOA fluxes is affected substantially by the changes in cloud cover occurring in the simulation. The changes in cloud cover are not, however, statistically significant, which makes it difficult to confirm the extent to which these changes occurred as a result of the aerosol radiative perturbation. Besides clouds, other reasons for the difference between model simulation and ERBE could be the lack of other actual forcings (e.g., QBO, ozone changes) in the model experiments. Because the period studied is of a limited duration, the atmosphere has gone through one realization, and the changes in climate parameters are generally small (except for the transient lower stratospheric warming), it is difficult to attribute quantitatively the degree to which different factors are responsible for the flux discrepancies between model and ERBE.

The temperature of the tropical lower stratosphere increases by a statistically significant 3 K, which is almost 1 K less than in earlier GCM simulations that were carried out with a coarser resolution of the stratosphere. The present result, though closer to observed values, is still higher. The lessening of the stratospheric response in the present work, compared to K99, is due to differences in cloud cover, an upward shifting of the maximum in aerosol heating (because of a higher vertical resolution), a more accurate radiation scheme, radiative cooling in middle and high altitudes, and a better resolution of the dynamical processes. In low latitudes the simulated temperature changes match the evolution in the observations, but with a positive bias, during most of the first year following the eruption. After spring 1992 there are discrepancies, with the QBO in the actual atmosphere (not accounted for in the model) probably being the major reason. Other factors that may not be negligible in causing differences between model and observations include ozone changes, tropospheric cloud cover changes, and other feedbacks.

Despite the fact that both the simulated magnitude and the evolution of the temperature response in the low latitudes depart from those observed about 9 months after the eruption, the global-mean lower stratospheric temperature response is in excellent agreement with the NCEP data over the entire 2-year period. This implies that (1) the input aerosol optical properties' evolution, and the corresponding evolution of the stratospheric radiative perturbations and model's temperature response are quite realistic, since the global-mean change is principally indicative of the model's sensitivity to an external radiative forcing; and (2) dynamical forcings and internal climate variability are large enough to yield a discrepancy, even in the tropics, where the aerosol optical depths remained high (0.25) through the end of 1992 and thus may have been expected to yield a signal large enough to be identified as being unambiguously due to the aerosols. In the high latitudes (poleward of 50°) the large interannual variability inhibits a clear

quantitative comparison and renders the aerosol-induced thermal signals statistically insignificant. Many more members in the ensemble may be needed to establish significance in these regions. However, because the atmosphere went through only one realization, there is a challenge in unambiguously identifying the aerosol-induced effects in the high-latitude lower stratosphere.

The global annual-mean warming in the lower stratosphere produced by the Pinatubo aerosols over the 2-year period is 0.3 K, while the cooling produced due to the 1979-1990 ozone depletion is about 0.12 K (scaled from the decadal changes to the 2-year period, assuming linearity). The net global- and annual-mean radiative forcing produced by the Pinatubo aerosols over the 2-year period is about 5 times larger than that due to the ozone loss (again, scaling in a linear manner for the 2-year period). Further, the spatial evolution of the simulated radiative forcing and lower stratospheric thermal response are different for these two species. Future work will address the dynamical changes and the tropospheric climate response, with an accounting of the QBO and observed ozone changes.

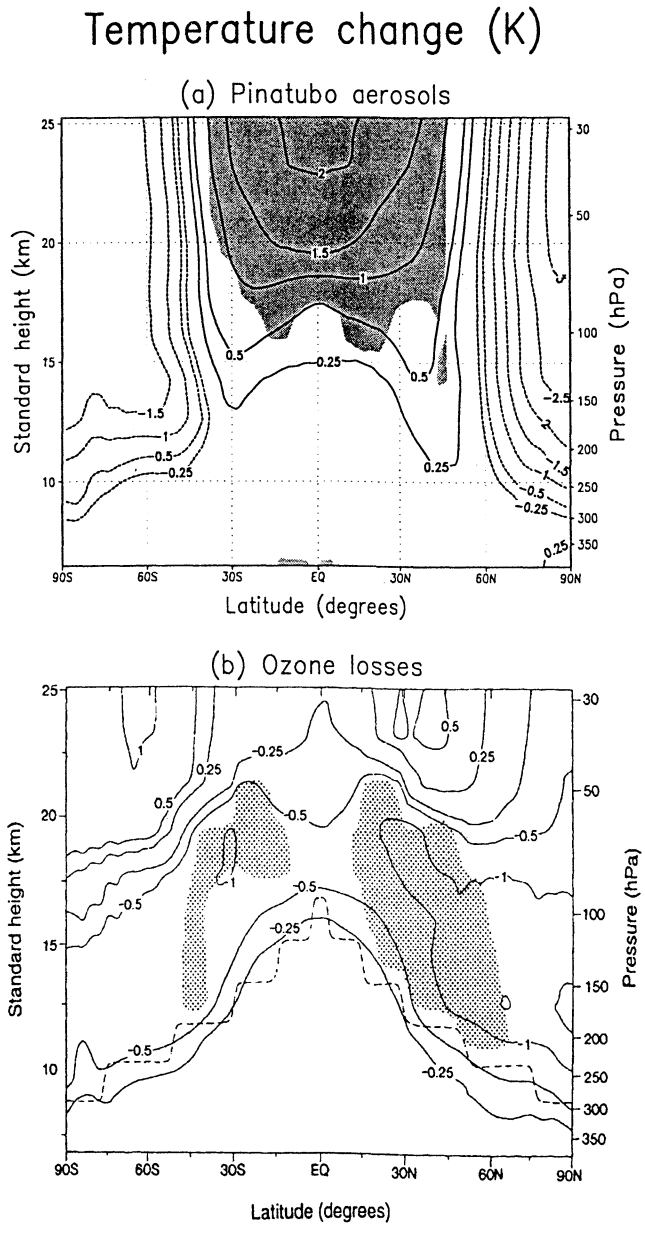


**Figure 11.** Annual mean temperature change (K) produced due to (a) Pinatubo aerosols, averaged for the 2-year period of the simulation, and (b) observed ozone loss for the 1979-1990 period, as simulated by the SKYHI GCM [*Ramaswamy et al.*, 1996]. Shaded areas denote statistical significance at the 99% significance level, as determined using a Student's *t*-test.

**Table 2.** Net Radiative (Solar+Longwave) Forcing (W $m^{-2}$) Produced by the Pinatubo Aerosols at the Tropopause Averaged for the Period of Simulation from June 1991 to May 1993 and Scaled for the 11-year Period (by Multiplying by 2/11) to be Compatible With the Forcing Due to the Observed Stratospheric Ozone Losses During 1979-1990 [*Ramaswamy et al.*, 1992] in Various Latitude Regions

| Latitude | Pinatubo Aerosols | Ozone |
|---|---|---|
| 90°-60°N | -0.06 | -0.15 |
| 60°-30°N | -0.25 | -0.13 |
| 30°-10°N | -0.51 | -0.04 |
| 10°N-10°S | -0.56 | 0.00 |
| 10°-30°S | -0.52 | 0.00 |
| 30°-60°S | -0.40 | -0.11 |
| 60°-90°S | -0.25 | -0.30 |
| Northern Hemisphere | -0.36 | -0.08 |
| Southern Hemisphere | -0.38 | -0.08 |
| Global | -0.37 | -0.08 |

**Acknowledgments.** We thank S. M. Freidenreich and M. D. Schwarzkopf for providing the new shortwave and longwave radiation codes and J. D. Mahlman for valuable discussions. We thank K. Hamilton, M. D. Schwarzkopf, and J. D. Mahlman for their comments on the manuscript. All the figures except Figure 4 are drawn with GrADS software, created by Brian Doty. We thank Patrick Minnis for providing the ERBE WFOV fluxes data and Melvyn Gelman for providing the FUB temperature data. Part of this work is supported by NSF grant ATM 99-96063 and NASA grant NAG 5-7913.

## References

Andronova, N. G., E. V. Rozanov, F. Yang, M. E. Schlesinger, and G. L. Stenchikov, Radiative forcing by volcanic aerosols from 1850 to 1994, *J. Geophys. Res.*, *104*, 16,807-16,826, 1999.

Angell, J. K., Estimated impact of Agung, El Chichon, and Pinatubo volcanic eruptions on global and regional total ozone after adjustment for the QBO, *Geophys. Res. Lett.*, *24*, 647-650, 1997a.

Angell, J. K., Stratospheric warming due to Agung, El Chichon, and Pinatubo taking into account the quasi-biennial oscillation, *J. Geophys. Res.*, *102*, 9479-9485, 1997b.

Barkstrom, B. R., The Earth Radiation Budget Experiment (ERBE), *Bull. Am. Meteorol. Soc.*, *65*, 1170-1185, 1984.

Bluth, G. J. S., S. D. Doiron, A. J. Krueger, L. S. Walter, and C. C. Schnetzler, Global tracking of the $SO_2$ clouds from the June 1991 Mount Pinatubo eruptions, *Geophys. Res. Lett.*, *19*, 151-154, 1992.

DeFoor, T. E., E. Robinson, and S. Ryan, Early observations of the June 1991 Pinatubo volcanic plume over Mauna Loa Observatory, Hawaii, *Geophys. Res. Lett.*, *19*, 187-190, 1992.

Deshler, T., B. J. Johnson, and W. R. Rozier, Balloonborne measurements of Pinatubo aerosol during 1991 and 1992 at 41°N: Vertical profiles, size distribution, and volatility, *Geophys. Res. Lett.*, *20*, 1435-1438, 1993.

Dutton, E. G., and J. R. Christy, Solar radiative forcing at selected locations and evidence for global lower tropospheric cooling following the eruptions of El Chichón and Pinatubo, *Geophys. Res. Lett.*, *19*, 2313-2316, 1992.

Fels, S. B., and L. D. Kaplan, A test of the role of longwave radiative transfer in a general circulation model, *J. Atmos. Sci.*, *33*, 779-789, 1975.

Fels, S. B., J. D. Mahlman, M. D. Schwarzkopf, and R.W. Sinclair, Stratospheric sensitivity to perturbations in ozone and carbon dioxide: Radiative and dynamical responses, *J. Atmos. Sci., 37*, 2265-2297, 1980.

Freidenreich, S. M, and V. Ramaswamy, A new multiple band solar radiative parameterization for GCMs, *J. Geophys. Res., 104*, 31,389-31,409, 1999.

Graf, H.-F., I. Kirchner, A. Robock, and I. Schult, Pinatubo eruption winter climate effects: Model versus observations, *Clim. Dyn., 9*, 81-93, 1993.

Grant, W. B., Tropical stratospheric ozone changes following the eruption of Mount Pinatubo, in *The Mount Pinatubo Eruption Effects on the Atmosphere and Climate, NATO ASI Ser.*, vol. I 42, edited by G. Fiocco, D. Fuà, and G. Visconti, pp. 161-175, Springer-Verlag, New York, 1996.

Hamilton, K., R. J. Wilson, J. D. Mahlman, and L.J . Umscheid, Climatology of the SKYHI troposphere-stratosphere-mesosphere general circulation model, *J. Atmos. Sci., 52*, 5-43, 1995.

Hansen, J. E., and A. A. Lacis, Sun and dust versus greenhouse gases, *Nature, 346*, 713-719, 1990.

Hansen, J. E., A. A. Lacis, and M. Sato, Potential climate impact of the Mount Pinatubo eruption, *Geophys. Res. Lett., 19*, 215-218, 1992.

Hansen, J. E., A. Lacis, R. Ruedy, M. Sato, and H. Wilson, How sensitive is the world's climate?, *Nat. Geogr. Res. Explor., 9*, 142-158, 1993.

Hansen, J., et al., A Pinatubo climate modeling investigation, in *The Mount Pinatubo Eruption Effects on the Atmosphere and Climate, NATO ASI Ser.*, vol. I 42, edited by G. Fiocco, D. Fuà, and G. Visconti, pp. 233-272, Springer-Verlag, New York, 1996.

Hansen, J. E., M. Sato, A. Lacis, and R. Ruedy, The missing climate forcing, *Phil. Trans. R. Soc. London. B, 352*, 231-240, 1997.

Harshvardhan, Perturbation of the zonal radiation balance by a stratospheric aerosol layer, *J. Atmos. Sci., 36*, 1274-1285, 1979.

Herman, J. R., and D. Larko, Low ozone amounts during 1992-1993 from Nimbus 7 and Meteor 3 total ozone mapping spectrometers, *J. Geophys. Res., 99*, 3483-3496, 1994.

Hofmann, D. J., and S. Solomon, Ozone destruction through heterogeneous chemistry following the eruption of El Chichón, *J. Geophys. Res., 94*, 5029-5041, 1989.

Houghton, J. T., L. G. Meira Filho, B. A. Callander, N. Harris, A. Kattenberg, and K. Maskell, (Eds.), *Climate Change 1995: The Science of Climate Change*, Cambridge Univ. Press, New York, 1996.

Jäger, H., O. Uchino, T. Nagai, T. Fujimoto, V. Freudenthaler, and F. Homburg, Ground-based remote sensing of the decay of the Pinatubo eruption cloud at three Northern Hemisphere sites, *Geophys. Res. Lett., 22*, 607-610, 1995.

Jayaraman, A., S. Ramachandran, Y. B. Acharya, and B. H. Subbaraya, Pinatubo volcanic aerosol layer decay observed at Ahmedabad (23°N), India, using neodymium: yttrium/aluminium/garnet backscatter lidar, *J. Geophys. Res., 100*, 23,209-23,214, 1995.

Joseph, J. H., W. Wiscombe, and J. A. Weinman, The delta-Eddington approximation for radiative flux transfer, *J. Atmos. Sci., 33*, 2452-2459, 1976.

Kalnay, E., et al., The NCEP/NCAR 40-year reanalysis project, *Bull. Am. Meteorol. Soc., 77*, 437-471, 1996.

King, M. D., and Harshvardhan, Comparative accuracy of selected multiple scattering approximations, *J. Atmos. Sci., 43*, 784-801, 1986.

Kinne, S., O. B. Toon, and M. J. Prather, Buffering of stratospheric circulation by changing amounts of tropical ozone: A Pinatubo case study, *Geophys. Res. Lett., 19*, 1927-1930, 1992.

Kirchner, I., G. L. Stenchikov, H.-F. Graf, A. Robock, and J. C. Antuña, Climate model simulation of winter warming and summer cooling following the 1991 Mount Pinatubo volcanic eruption, *J. Geophys. Res., 104*, 19,039-19,055, 1999.

Kodera, K., Influence of volcanic eruptions on the troposphere through stratospheric dynamical processes in the Northern Hemisphere winter, *J. Geophys. Res., 99*, 1273-1282, 1994.

Labitzke, K., Stratospheric temperature changes after the Pinatubo eruption, *J. Atmos. Terr. Phys., 56*, 1027-1034, 1994.

Labitzke, K., and H. van Loon, A note on the distribution of trends below 10 hPa: The extratropical Northern Hemisphere, *J. Meteorol. Soc. Jpn., 73*, 883-889, 1995.

Lacis, A., J. E. Hansen, and M. Sato, Climate forcing by stratospheric aerosols, *Geophys. Res. Lett., 19*, 1607-1610, 1992.

Lambert, A., R. G. Grainger, J. J. Remedios, C.D. Rodgers, M. Corney, and F. W. Taylor, Measurements of the evolution of the Mount Pinatubo aerosol cloud by ISAMS, *Geophys. Res. Lett., 20*, 1287-1290, 1993.

Li, J., and V. Ramaswamy, Four-stream spherical harmonic expansion approximation for solar radiative transfer, *J. Atmos. Sci., 53*, 1174-1186, 1996.

Long, C. S., and L. L. Stowe, Using the NOAA/AVHRR to study stratospheric aerosol optical thicknesses following the Mount Pinatubo eruption, *Geophys. Res. Lett., 21*, 2215-2218, 1994.

Mahlman, J. D., and L. J. Umscheid, Dynamics of the middle atmosphere: Successes and problems of the GFDL SKYHI general circulation model, in *Dynamics of the Middle Atmosphere*, edited by J. R. Holton and T. Matsuno, pp. 501-525, Terra Sci., Tokyo, 1984.

Mahlman, J. D., J. P. Pinto, and L. J. Umscheid, Transport, radiative, and dynamical effects of the Antarctic ozone hole: A GFDL SKYHI model experiment, *J. Atmos. Sci., 51*, 489-508, 1994.

McCormick, M. P., and R. E. Veiga, SAGE II measurements of early Pinatubo aerosols, *Geophys. Res. Lett., 19*, 155-158, 1992.

Minnis, P., E. F. Harrison, L. L. Stowe, G. G. Gibson, F. M. Denn, D. R. Doeling, and W. L. Smith Jr., Radiative climate forcing by the Mount Pinatubo eruption, *Science, 259*, 1411-1415, 1993.

Mohnen, V. A., Stratospheric ion and aerosol chemistry and possible links with cirrus cloud microphysics—A critical assessment, *J. Atmos. Sci., 47*, 1933-1948, 1990.

Palmer, K. F., and D. Williams, Optical constants of sulfuric acid: Application to the clouds of Venus, *Appl. Opt., 14*, 208-219, 1975.

Ramanathan, V., and R. E. Dickinson, The role of stratospheric ozone in the zonal and seasonal radiative energy balance of the Earth-troposphere system, *J. Atmos. Sci., 36*, 1084-1104, 1979.

Ramaswamy, V., and M. Bowen, Effect of radiatively active species upon the lower stratospheric temperatures, *J. Geophys. Res., 99*, 18,909-18,921, 1994.

Ramaswamy, V., M. D. Schwarzkopf, and K. P. Shine, Radiative forcing of climate from halocarbon-induced global stratospheric ozone loss, *Nature, 355*, 810-812, 1992.

Ramaswamy, V., M. D. Schwarzkopf, and W. J. Randel, Fingerprint of ozone depletion in the spatial and temporal pattern of recent lower-stratospheric cooling, *Nature, 382*, 616-618, 1996.

Randel, W. J., F. Wu, J. M. Russell III, J. W. Waters, and L. Froidevaux, Ozone and temperature changes in the stratosphere following the eruption of Mount Pinatubo, *J. Geophys. Res., 100*, 16,753-16,764, 1995.

Robock, A., Volcanic eruptions and climate, *Rev. Geophys., 38*, 191-219, 2000.

Robock, A., and J. Mao, Winter warming from large volcanic eruptions, *Geophys. Res. Lett., 12*, 2405-2408, 1992.

Robock, A., and J. Mao, The volcanic signal in surface temperature observations, *J. Clim., 8*, 1086-1103, 1995.

Robock, A., K. E. Taylor, G. L. Stenchikov, and Y. Liu, GCM evaluation of a mechanism for El Niño triggering by the El Chichón ash cloud, *Geophys. Res. Lett., 22*, 2369-2372, 1995.

Roeckner, E., K. Arpe, L. Bengsston, M. Christoph, M. Claussen, L. Duemenil, M. Esch, M. Giorgetta, U. Schlese, and U. Schulzweida, *The Atmospheric General Circulation Model ECHAM4: Model Description and Present-Day Climate*, Tech. rep. 218, 90 pp., Max Planck Inst. for Meteorol., Hamburg, Germany, 1996.

Russell, P. B., et al., Pinatubo and pre-Pinatubo optical depth spectra: Mauna Loa measurements, comparisons, inferred particle size distributions, radiative effects, and relationship to lidar data, *J. Geophys. Res., 98*, 22,969-22,985, 1993.

Russell, P. B., et al., Global to microscale evolution of the Pinatubo volcanic aerosol, derived from diverse measurements and analyses, *J. Geophys. Res., 101*, 18,745-18,763, 1996.

Santer, B. D., J. J. Hnilo, T. M. L. Wigley, J. S. Boyle, C. Doutriaux, M. Fiorino, D. E. Parker, and K. E. Taylor, Uncertainties in observationally based estimates of temperature change in the free atmosphere, *J. Geophys. Res., 104*, 6305-6333, 1999.

Sassen, K., D. O. Starr, G. G. Mace, M. R. Poellot, S. H. Melfi, W. L. Eberhard, J. D. Spinhirne, E. W. Eloranta, D. E. Hagen, and J. Hallett, The 5-6 December 1991 FIRE IFO II jet stream cirrus case study: Possible influences of volcanic aerosols, *J. Atmos. Sci., 52*, 97-123, 1995.

Schoeberl, M. R., P. K. Bhartia, and E. Hilsenrath, Tropical ozone loss following the eruption of Mount Pinatubo, *Geophys. Res. Lett., 20*, 29-32, 1993.

Schwarzkopf, M. D., and S. B. Fels, The simplified exchange method revisited: An accurate, rapid method for computation of infrared cooling rates and fluxes, *J. Geophys. Res.*, *96*, 9075-9096, 1991.

Schwarzkopf, M. D., and V. Ramaswamy, Radiative effects of $CH_4$, $N_2O$, halocarbons, and the foreign-broadened $H_2O$ continuum: A GCM experiment, *J. Geophys. Res.*, *104*, 9467-9488, 1999.

Shibata, K., O. Uchino, T. Kamiyama, and M. P. McCormick, An estimation of the radiative effect in the stratosphere due to the Pinatubo aerosol, *J. Meteorol. Soc. Jpn.*, *74*, 763-780, 1996.

Shibata, T., T. Itabe, K. Mizutani, and K. Asai, Pinatubo volcanic aerosols observed by lidar at Wakkanai, Japan, *Geophys. Res. Lett.*, *21*, 197-200, 1994.

Shindell, D. T., R. L. Miller, G. A. Schmidt, and L. Pandolfo, Simulation of recent northern winter climate trends by greenhouse-gas forcing, *Nature*, *399*, 452-455, 1999.

Slingo, A., A GCM parameterization of the shortwave radiative properties of water clouds, *J. Atmos. Sci.*, *46*, 1419-1427, 1989.

Solomon, S., Stratospheric ozone depletion: A review of concepts and history, *Rev. Geophys.*, *37*, 275-316, 1999.

Solomon, S., R. W. Portmann, R. R. Garcia, L. W. Thomason, L. R. Poole, and M. P. McCormick, The role of aerosol variations in anthropogenic ozone depletion at northern midlatitudes, *J. Geophys. Res.*, *101*, 6713-6727, 1996.

Stenchikov, G. L., I. Kirchner, A. Robock, H.-F. Graf, J. C. Antuña, R. G. Grainger, A. Lambert, and L. W. Thomason, Radiative forcing from the 1991 Mount Pinatubo volcanic eruption, *J. Geophys. Res.*, *103*, 13,837-13,857, 1998.

Stowe, L. L., R. M. Carey, and P. P. Pellegrino, Monitoring the Mount Pinatubo aerosol layer with NOAA/11 AVHRR data, *Geophys. Res. Lett.*, *19*, 159-162, 1992.

Thompson, D. W. J., and J. M. Wallace, The Arctic Oscillation signature in the wintertime geopotential height and temperature fields, *Geophys. Res. Lett.*, *25*, 1297-1300, 1998.

Timmreck, C., H.-F. Graf, and I. Kirchner, A one and a half year interactive MA/ECHAM4 simulation of Mount Pinatubo aerosol, *J. Geophys. Res.*, *104*, 9337-9359, 1999.

Trepte, C. R., R. E. Veiga, and M. P. McCormick, The poleward dispersal of Mount Pinatubo volcanic aerosol, *J. Geophys. Res.*, *98*, 18,563-18,573, 1993.

Turco, R. P., K. Drdla, A. Tabazadeh, and P. Hamill, Heterogeneous chemistry of polar stratospheric clouds and volcanic aerosols, in *The Role of the Stratosphere in Global Change*, edited by M.-L. Chanin, pp. 65-134, NATO ASI Ser., vol. 8, Springer-Verlag, New York, 1993.

Wetherald, R. T., and S. Manabe, Cloud feedback processes in a general circulation model, *J. Atmos. Sci.*, *45*, 1397-1415, 1988.

World Meteorological Organization (WMO), Report of the International Ozone Trends Panel 1988, *WMO Rep. 18*, Global Ozone Res. and Monit. Project, Geneva, 1990.

Yang, F., M. E. Schlesinger, and E. Rozanov, Description and performance of the UIUC 24-layer stratosphere/troposphere general circulation model, *J. Geophys. Res.*, *105*, 17,925-17,954, 2000.

Young, R. E., H. Houben, and O. B. Toon, Radiatively forced dispersion of the Mount Pinatubo volcanic cloud and induced temperature perturbations in the stratosphere during the first few months following the eruption, *Geophys. Res. Lett.*, *21*, 269-372, 1994.

S. Ramachandran, Planetary Atmospheric Sciences Division, Physical Research Laboratory, Navrangpura, Ahmedabad 380 009, India. (ram@prl.ernet.in)

V. Ramaswamy, NOAA Geophysical Fluid Dynamics Laboratory, P.O. Box 308, Princeton, NJ 08542-0308. (vr@gfdl.gov)

A. Robock (corresponding author) and G. L. Stenchikov, Department of Environmental Sciences, Rutgers University, 14 College Farm Road, New Brunswick, NJ 08901-8551. (robock@envsci.rutgers.edu; gera@envsci.rutgers.edu)

(Received February 8, 2000; revised May 22, 2000;
accepted May 31, 2000.)